FINAL REPORT

High Pressure Laser Plasma Studies

NASA Grant NSG 1383

Principal Investigator

W. E. Wells
Associate Professor
Department of Physics
Miami University
Oxford, Ohio 45056

CONTENTS

Section		Page
I.	INTRODUCTION	1
II.	THEORY	3
III.	EXPERIMENTAL PROCEDURES AND EQUIPMENT	9
IV.	EXPERIMENTAL RESULTS	22
APPENDIX I		36
APPENDIX II		52
REFERENCES		60

I. INTRODUCTION

A nuclear pumped laser, operating at a wavelength of 1.79 μm. on the 3d(1/2)-4p(3/2) transition in argon with ^3He as the majority gas has been produced by Jalufka et. al. at NASA-Langley Research center.[1] A model, proposed by Harries and Wilson, to explain the operation of this laser uses collisional radiative recombination of Ar^+ as the population mechanism of the 3d(1/2) state.[2] This model also proposes dissociative recombination of Ar_2^+ as a population mechanism for the 4p(3/2) state.

Work done by Biondi et. al. at the University of Pittsburgh confirms that dissociative recombination populates the 4p level but indicates that dissociative recombination dominates over collisional radiative recombination in pure argon at low pressures.[3] As the laser developed at NASA-Langley operates in the high-pressure regime, calculations have been performed by DePaola et. al. (see Appendix 1) extrapolating well-known low-pressure results to the high-pressure regime. From the results of these calculations there is some question in predicting laser operation at 1.79 μm. in a ^3He-Ar plasma[9].

The purpose of this study is the investigation of the

energy pathways in He-Ar gas mixtures at low pressure is accomplished by observing the effects of varying partial pressures on the emissions of levels lying above the 4p level in argon during a pulsed afterglow. An attempt was made to investigate the population mechanisms of the 3d level in pure argon by observing emission from the 3d(1/2)-4p(3/2) transition in a high-pressure plasma excited by a high-energy electron beam.

II. THEORY

A nuclear pumped, ^3He-Ar laser, excited by the $^3He(n,p)^3H$ reaction, was created by Jalufka et. al. in 1976.[1] The laser operates at a wavelength of 1.79 μm. on the 3d(1/2)-4p(3/2) transition in atomic argon. A model for the laser, proposed by Harries and Wilson, assumes that the population mechanism of the 3d(1/2) state is collisional radiative recombination of Ar^+ and that dissociative recombination of Ar_2^+ populates the 4p(3/2) state.[2]

A flow diagram, illustrating the energy pathways proposed, is shown in figure 1. The greater part of the fission energy produces helium ions, He^+, and excited helium atoms in a metastable state, $He(2^3S)$. Some of the $He(2^3S)$ is converted to a molecular helium metastable, $He_2(2^3\Sigma)$. Argon ions are created from both atomic and molecular helium metastables by Penning ionization. The helium ions are converted to molecular helium ions, He_2^+, which also serve to ionize the argon by charge transfer collisions. The ionic argon may recombine by collisional radiative recombination or be converted to Ar_2^+. The products of collisional radiative recombination cascade through excited states and may produce a population inversion between the 3d(1/2) and 4p(3/2) states. Molecular argon ions undergo dissociative recombination which

Figure 1. Flow Diagram of Processes Important to the ^{3}He-Ar Laser.

Dissociative recombination is assumed to populate the lower laser level.

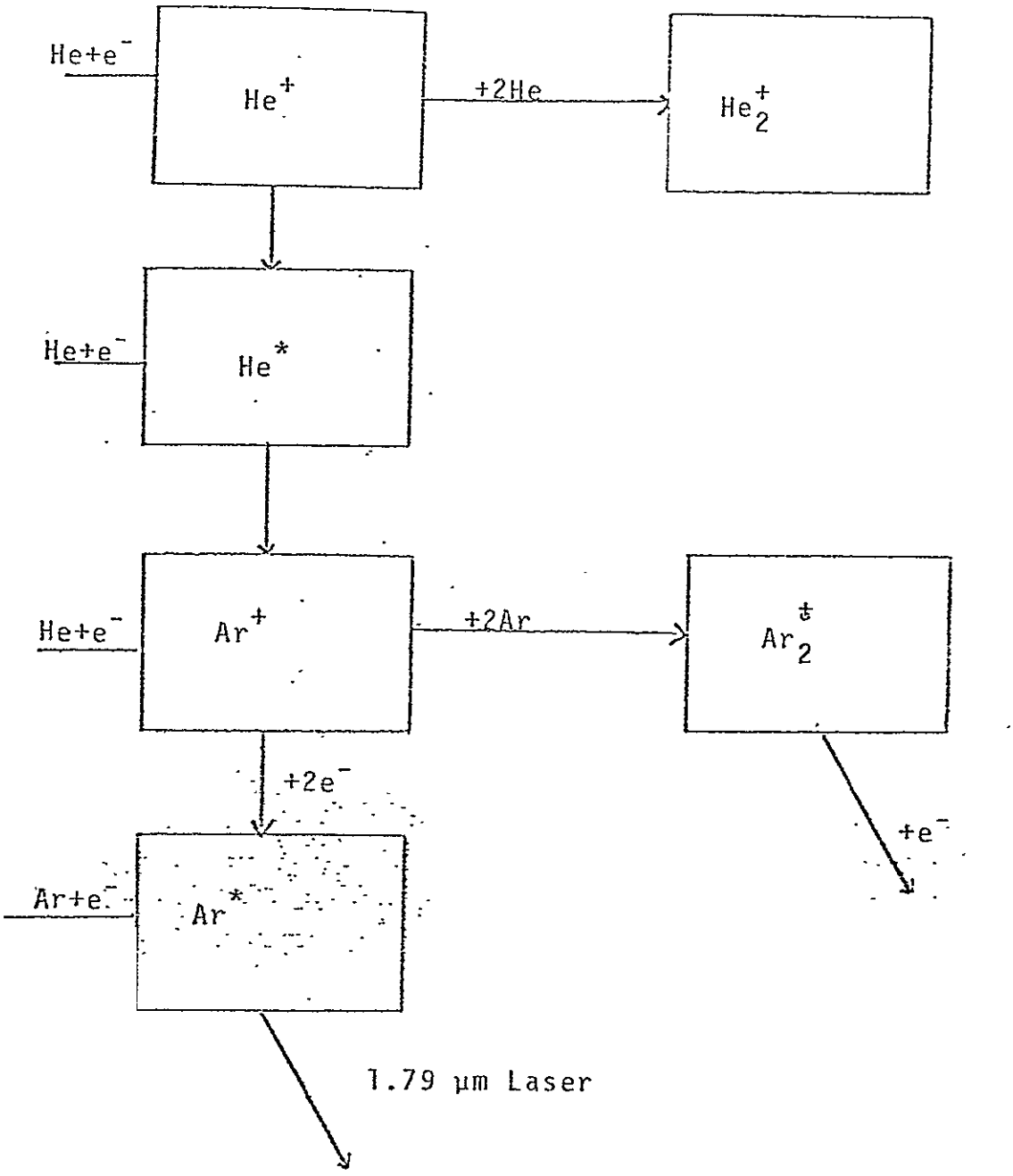
He+e⁻
He⁺
+2He
He₂⁺
He+e⁻
He*
He+e⁻
Ar⁺
+2Ar
Ar₂*
+2e⁻
+e⁻
Ar+e⁻
Ar*
1.79 μm Laser

is presumed to populate the 4p(3/2) state thus becoming a source of population for the lower laser level.

The assumption that dissociative recombination populates the lower laser level is supported by the work of Biondi ans Shiu which shows that the 4p states are the most strongly populated.[3] Experiments performed by Frommhold and Biondi, in 1969, indicate that dissociative recombination dominates over collisional radiative recombination in pure argon at low pressure.[4]

Calculations performed by DePaola et. al. (see Appendix 1) provide a characterization of high-pressure ^{3}He-Ar plasmas based on extrapolation of the knowledge of similar low-pressure plasmas.[9] Results of these calculations for a ^{3}He-Ar plasma at a total pressure of 2 atmospheres with a 1% concentration of argon and a thermal neutron flux of 10^{18} neutrons-cm^{-2}-sec^{-1} are quoted here:

Gas Temperature	T_o=300 K
Electron Temperature	T_e=536 K
Electron Density	$N_e=2.08X10^{14}$ cm^{-3}
Ar^+ Density	$\{Ar^+\}=7.57X10^{13}$ cm^{-3}
Ar_2^+ Density	$\{Ar_2^+\}=1.08X10^{14}$ cm^{-3}.

Collisional radiative rate coefficients for the minority gases in various helium-dominated gas mixtures have been calcuated by Whitten et. al.[5] For a He-Ar mixture at 2 atmospheres total pressure the rate coefficient is:

$$\alpha_{CRR}=2.55X10^{-9} \text{ cm}^{+3}\text{-sec}^{-1}$$

and the rate coefficient for dissociative recombination of Ar_2^+ is:

$$\alpha_D=9.1X10^{-7}(T_e/T_o)^{-.61} \text{ cm}^3\text{-sec}^{-1}$$

The assumption may be made that all of the products of collisional radiative recombination pass through the 3d level and are distributed according to the densities of the individual states within the level. The same assumption is made with respect to the products of dissociative recombination cascading through the 4p level. The rates of poulation of the two states are thus:

$$d\{Ar(3d(1/2))\}/dt=2/20X\alpha_{CRR}\{Ar^{+}\}N_e$$
$$=4.02X10^{18}\ cm^{-3}\text{-}sec^{-1}$$

$$d\{Ar(4p(3/2))\}/dt=4/12X\alpha_{D}\{Ar_2^{+}\}N_e$$
$$=4.78X10^{21}\ cm^{-3}\text{-}sec^{-1}$$

The rate of population of the lower laser level is thus seen to be three orders of magnitude greater than that of the upper laser level and laser action is not predicted in this model.

The characteristics of an existing ^{3}He-Ar laser may be used to predict the value of the collisional radiative recombination rate coefficient necessary to produce lasing. A laser described by DeYoung et. al. operates at 2 atmospheres total pressure with a 1% argon concentration.[6] The peak power output of the laser is 3.4 Watts for a thermal neutron flux of 10^{17} neutrons-cm^{-2}-sec^{-1}. The efficiency of the laser is reported to be 0.09%. The power deposited in a laser of this type is:

$$\xi_i=\sigma\phi\{^3He\}E_FV$$

where $\sigma=5X10^{-21}$ cm^2 is the fission cross-section of ^{3}He, ϕ is the thermal neutron flux, $E_F=0.79$ Mev is the energy released per fission event and V is the active volume. The

power output is given by:

$$\xi_0 = \varepsilon \xi_i$$

$$= \varepsilon \sigma \phi \{^3He\} E_F V$$

where ε is the efficiency of the laser. Thus the active volume is given by:

$$V = \xi_o / \varepsilon \sigma \phi \{^3He\} E_F$$

$$= 1.162 \text{ cm}^3$$

The peak power output of 3.4 Watts corresponds to 3.06×10^{19} photons-sec^{-1} at 1.79 μm. As the ^{3}He-Ar laser is a steady-state laser the source term for the population of the 3d(1/2) state must be equal to the loss term. Using the model of Harries and Wilson this requirement becomes:

$$\alpha_{CRR} N_e \{Ar^+\} V = 3.06 \times 10^{19}$$

or:

$$\alpha_{CRR} = 3.06 \times 10^{19} / N_e \{Ar^+\} V$$

The computer program used by DePaola et. al. was modified slightly (see Appendix 2) to calculate the electron and ion densities of a ^{3}He-Ar plasm at 2 atmospheres with a thermal neutron flux of 10^{17} neutrons-cm^{-2}-sec^{-1}. The results are:

Electron Density $N_e = 5.53 \times 10^{13}$ cm^{-3}

Ar^+ Density $\{Ar+\} = 1.81 \times 10^{13}$ cm^{-3}

And the required collisional radiative rate coefficient is:

$$\alpha_{CRR} = 2.63 \times 10^{-8}$$

a full order of magnitude greater than that calculated by Whitten et. al.[5]

III. EXPERIMENTAL PROCEDURES AND EQUIPMENT

The gas mixtures of interest in this study were excited by a pulsed electrical discharge. Pulse duration was 4.5 ±.05 μsec with a peak current of 40±5 amps (see figure 7). Electrode spacing was 7.5 cm in a glass discharge tube with quartz windows. The discharge tube was 2.5 cm in diameter and 1 m long

Figure 2 shows a block diagram of the vacuum and gas-handling system. The pumping system consists of a 4-inch oil diffusion pump with a liquid nitrogen cold trap and auxiliary roughing pump. The diffusion pump was capable of bringing the entire gas-handling system to a pressure of 10^{-7} Torr and the discharge tube was brought to a pressure of 10^{-5} Torr or better prior to each gas fill.

The gas inlet system consisted of reservoirs of research grade helium and argon with controlled-flow valves connected to the remainder of the system through a length of 1/4-inch copper tubing. Gas pressure was monitored by an absolute

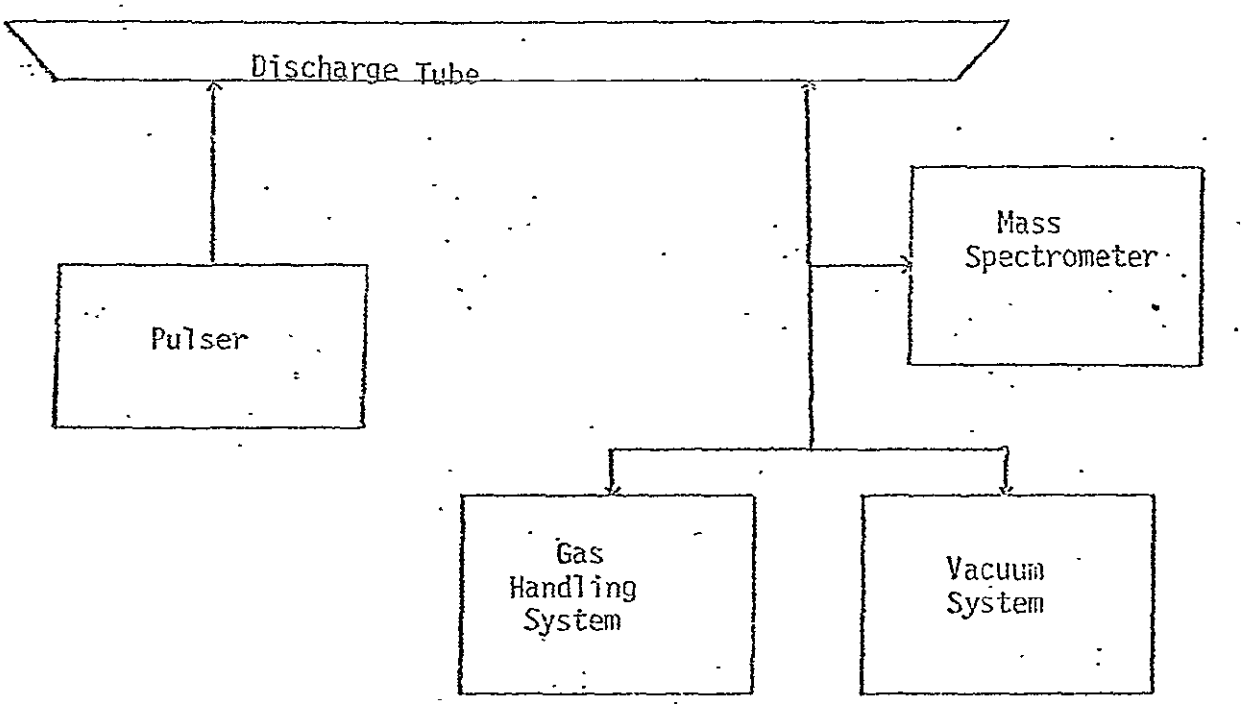

Figure 2. Block Diagram of Vacuum and Gas-Handling System.

pressure gauge calibrated from 0.1 to 20 Torr in 0.1 Torr gradations and a differential gauge calibrated from 0 to 800 Torr in 10 Torr gradations attached to the gas inlet system. Under vacuum conditions pressure could be monitored by the mass spectrometer or by an ionization guage (Varian model 563) calibrated from 10^{-4} to 10^{-8} and attached to the gas chamber.

Preparation of Gas Mixtures

In preparing the gas mixtures to be studied the entire system was first flushed with the minority gas to reduce impurity levels. The minority gas was used in flushing as insurance against possible incomplete pumping due to the low conductance of the 1/4-inch tubing used in the gas inlet system. Following this the discharge tube was overpressured with the desired gas mixture and subsequently pumped to 10 Torr. Before each run the discharge tube was isolated from the vacuum and gas-handling system.

Data Aquisition System

The data aquisition system is shown schematically in figure 3. Data was accumulated by a photomultiplier tube (RCA model 7625) attached to a 0.5-meter Ebert scanning spectrometer (Jarrel-Ash model 82-000). The spectrometer was calibrated to within 5 angstroms with a mercury arc lamp and location of individual lines was verified by maximizing the signal

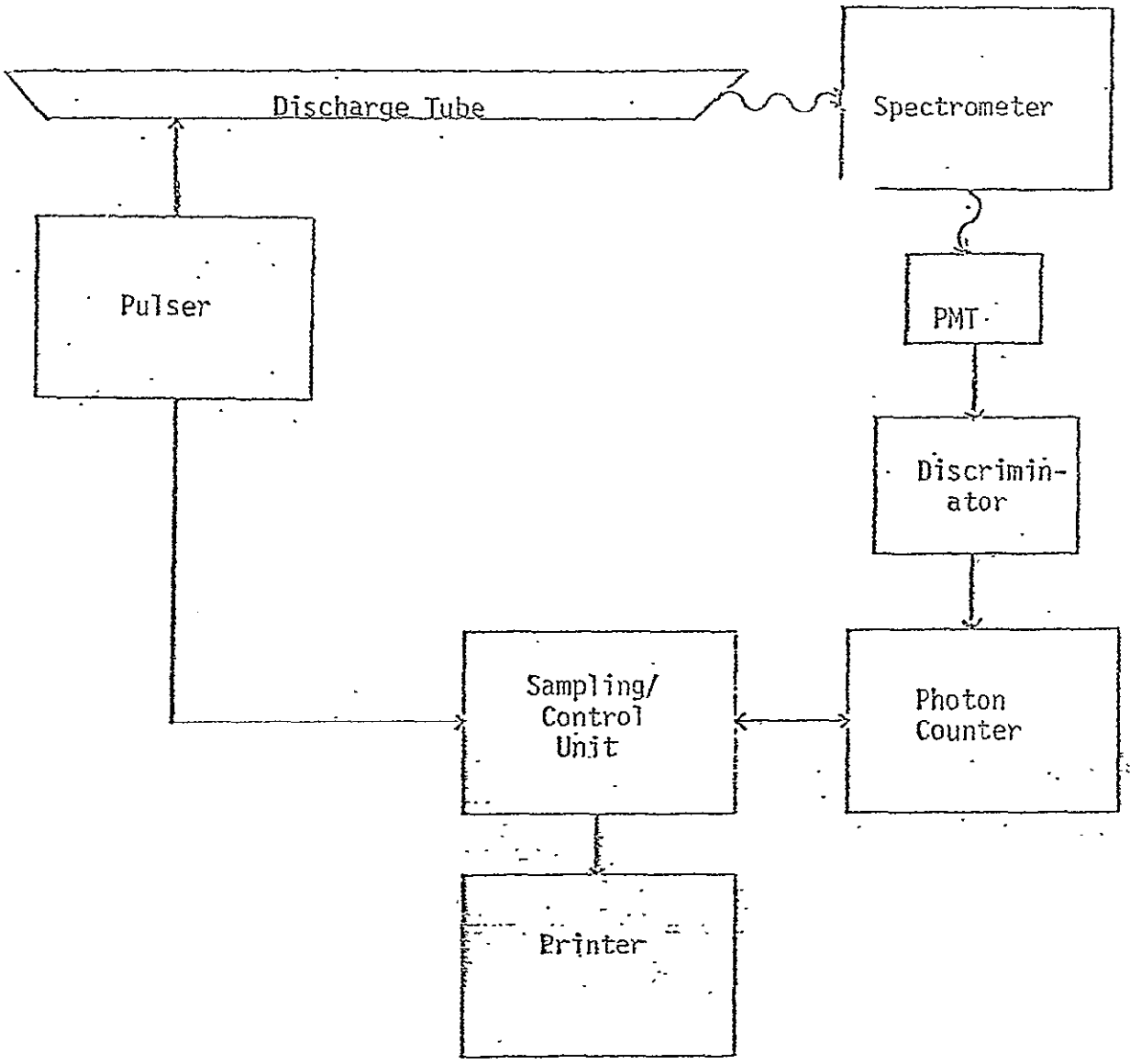

Figure 3. Block Diagram of Data Aquisition System.

The signal from the PMT was routed through a photon Discriminator/Amplifier before going to the photon counter.

from the photomultiplier as viewed on an oscilloscope. The photomultiplier signal was then routed to a photon discriminator/amplifier (Mech-Tronics model 511) to a photon counting system.

The photon counting system consisted of a photon counter (Ortec model 9315) with a sampling/control unit (Ortec model 9320). The photon counting system was operated in a 30-step boxcar mode allowing counting to take place during a preselected time period at 30 different temporal positions in the active discharge and afterglow[7] (see figure 4). A pretrigger was supplied to the sampling/control unit by the discharge power supply trigger 1 msec before the initiation of the current pulse. A variable delay line in the sampling/control unit served to initiate counting approximately 20 μsec in advance of the current pulse for each cycle. During step 1 the photon counter is enabled by a 40 μsec gate signal supplied by the sampling/control unit. This is repeated for each trigger pulse received by the sampling/control unit for the duration of an integration interval of 5000 current pulses. At the end of the integration interval the data accumulated by the photon counter is transferred to a buffer where it is available for recording. The delay to the gate signal is then incremented by twice the selected gate width and step 2 begins. Operation during step 2 is identical to that of step 1 except that counting begins at a later time in the discharge/afterglow. A gate width of 40 μsec gave samples as far as 2.4 msec into the afterglow. An integration interval of 200 sec yielded over 5000 current pulses

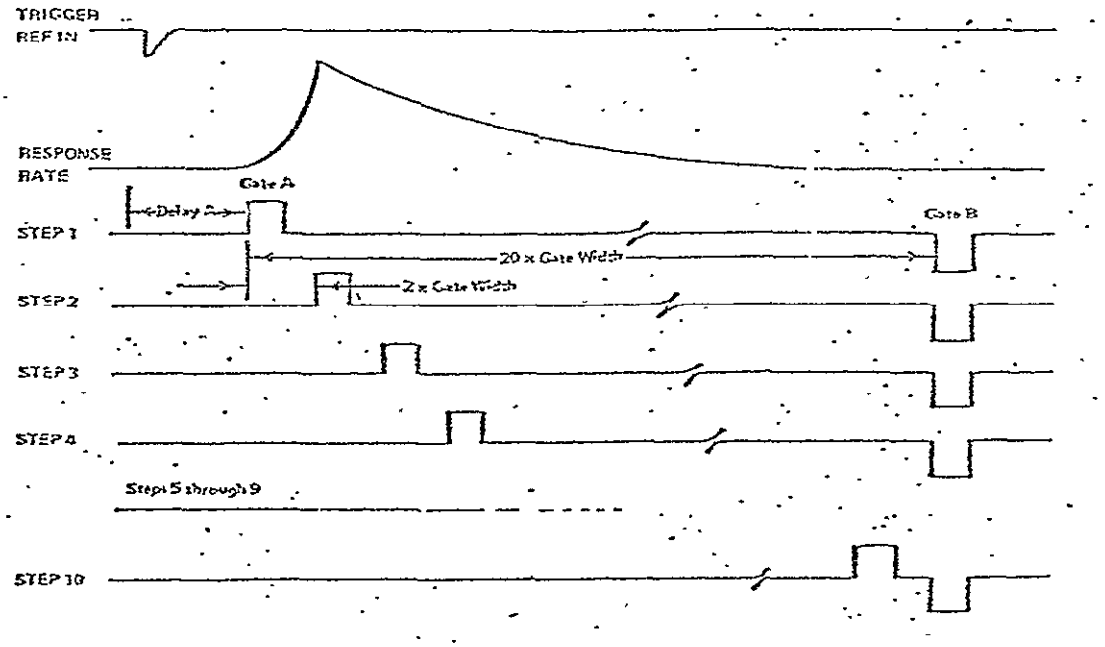

Figure 4 Schematic of Timing for the Photon Counting System. The gate signal in step 1 began 20μsec before the current pulse.

from a pulse rate of 25 sec^{-1}.

Calibration of the Optical System

The spectral response of the spectrometer and photomultiplier tube was calibrated with a tungsten filament lamp (ITT model T-10) placed behind the discharge tube. The temperature of the filament was 1500 K. The spectrum of the lamp, corrected for the self-absorption of the filament, is shown in figure 5 and the spectral response of the optical system is shown in figure 6. The response curve shows the signal from the photomultiplier tube, as a function of wavelenth, relative to the response at 3600 angstroms.

Electron Beam System

The system used for high-pressure measurements is shown schematically in figure 7. It consists of an electron beam machine supplied by Maxwell Research Co. attached to a stainless steel plasma cell 28.5 inches long and 12 inches in diameter. Two CaF_2 windows, 2 inches in diameter, were attached to the cell at its midpoint. The electron beam delivered approximately 7.5 amps-cm^{-2} at 60 kV in 900 nsec pulses. The gas-handling system and preparation procedures were similar to those described above with the exception of the total pressures. A pressure of 300 Torr was used for the electron beam measurements. Data was accumulated by a liquid nitrogen-cooled InAs infrared detector (Barnes Engineering model 0211) attached to the same spectrometer described above. The spectrometer was equipped with an infrared grating (Jarrel-

Figure 5 Spectral Response of Calibration Lamp. Blackbody curve of a tungsten filament at 1500 corrected for self-absorption. Intensity is arbitrary units.

SPECTRAL RESPONSE OF CALIBRATION LAMP

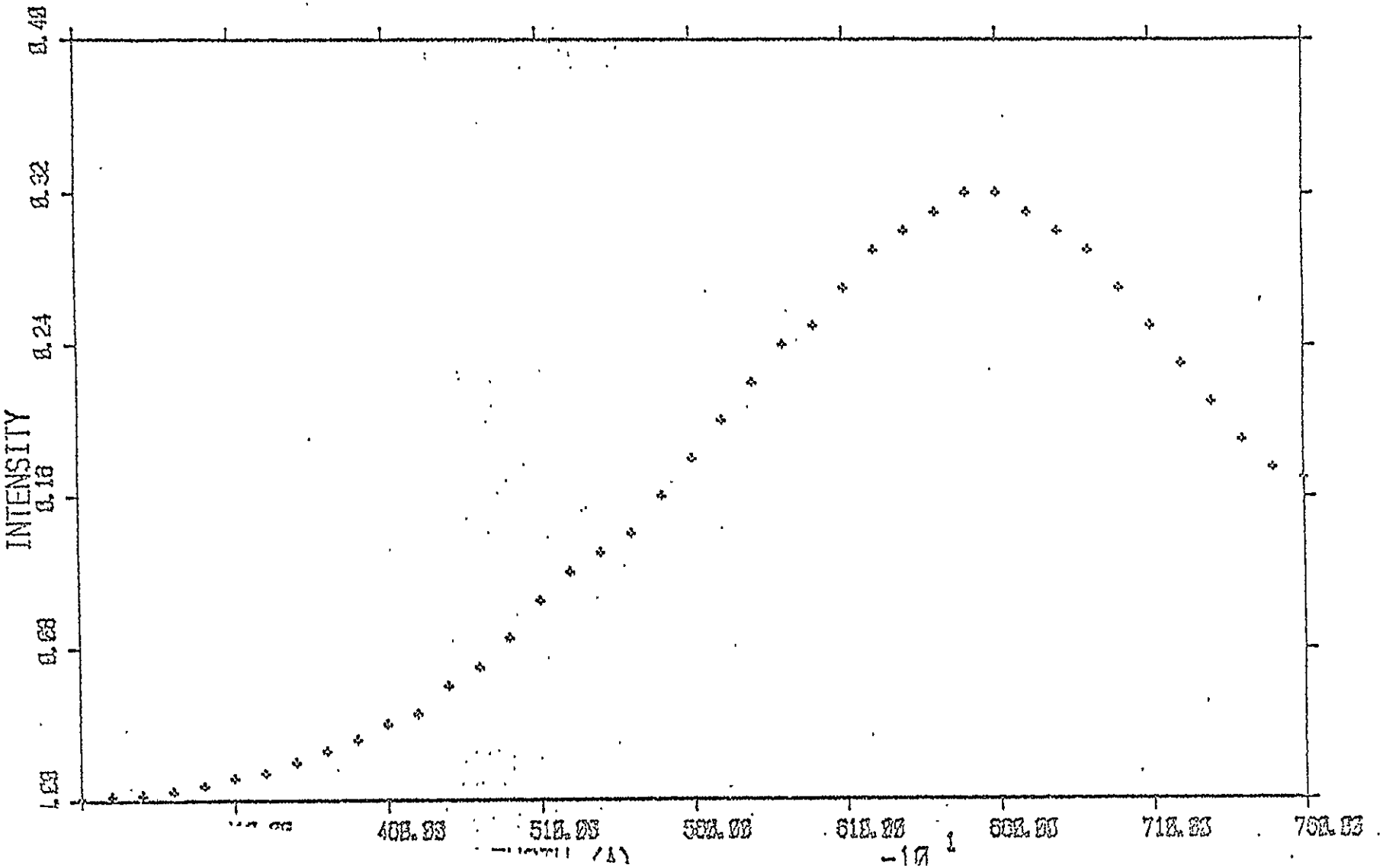

Figure 6 Spectral Response of the Optical System.

Response relative to the response at 3600 angstroms is shown.

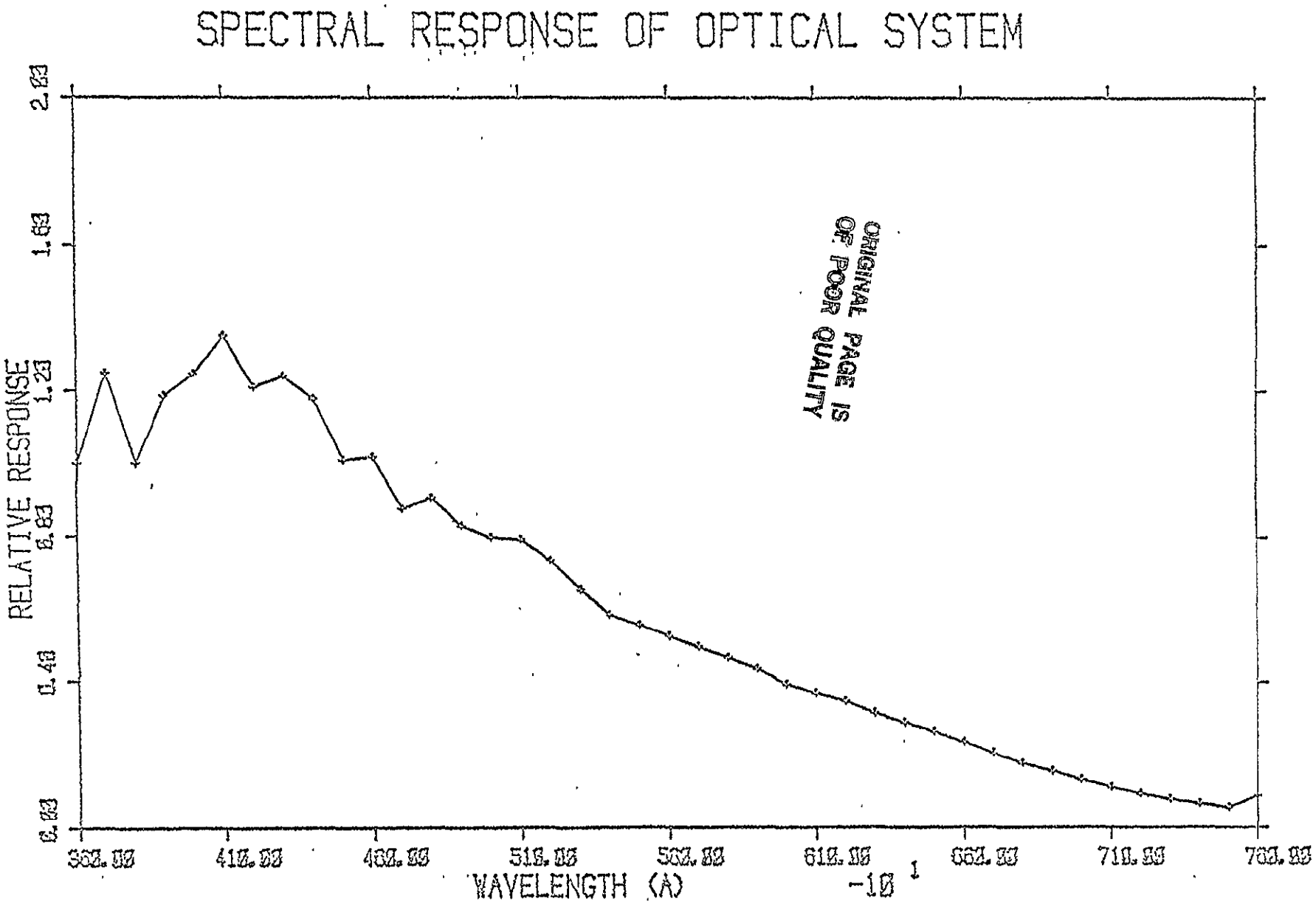
SPECTRAL RESPONSE OF OPTICAL SYSTEM
RELATIVE RESPONSE
2.03
1.63
1.23
0.83
0.43
363.00
413.00
463.00
513.00
563.00
613.00
663.00
713.00
763.00
WAVELENGTH (A)
-10 1
ORIGINAL PAGE IS
OF POOR QUALITY

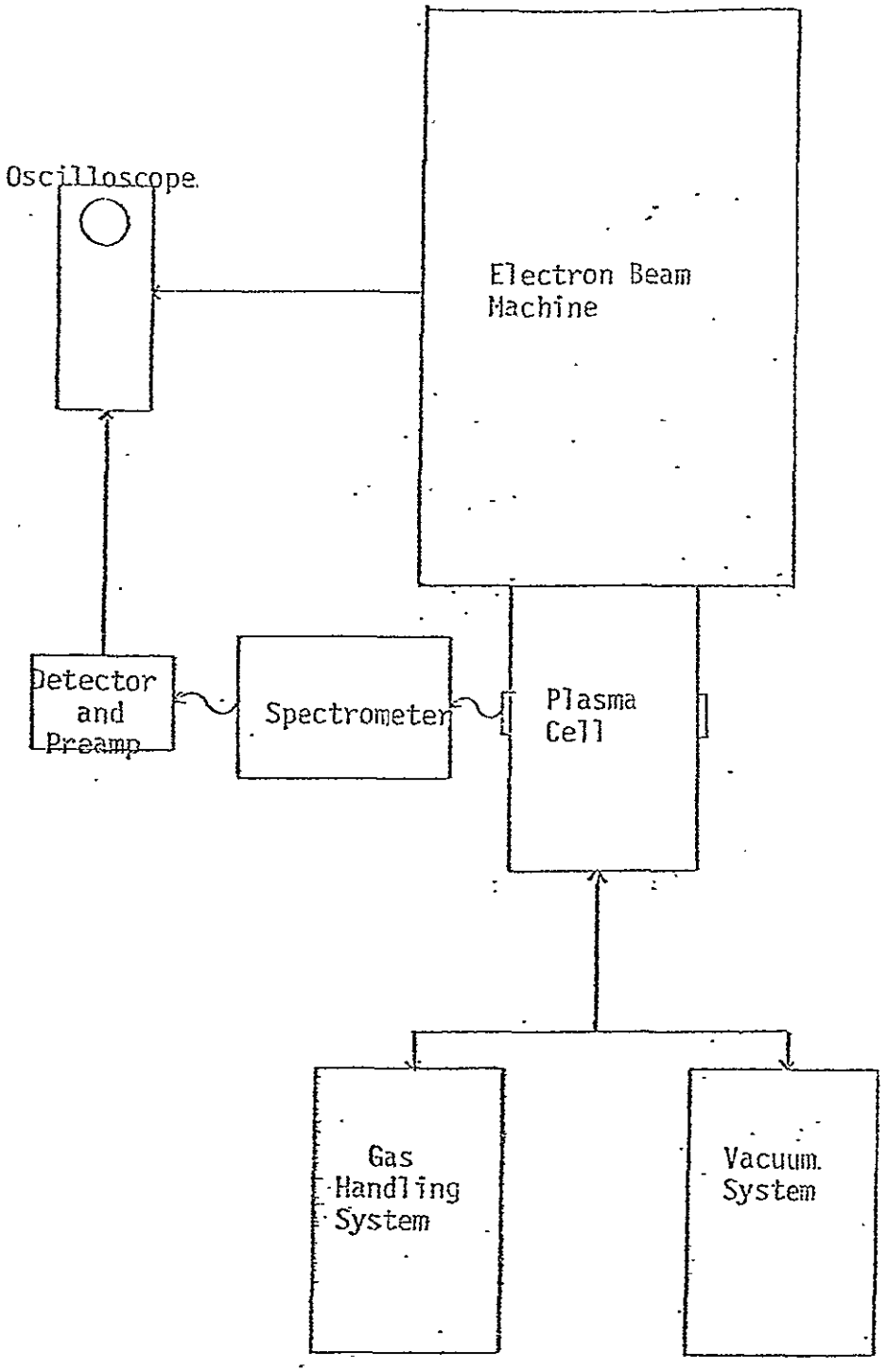

Figure 7 .. Block Diagram Showing High-Pressure Apparatus.

Ash #1347D8A9). The signal from the detector was amplified by a 60-db gain low-noise preamplifier (Ortec model 7506) and viewed directly on an oscilloscope (Tektronix model 466) in storage mode.

IV. EXPERIMENTAL RESULTS

The results of this study are presented in three sections. First, the intensities of observed emission lines are presented. A quantitative discussion of the results is presented in the second section. This is followed by a summary of the conclusions drawn from this work.

Intensities of Some emission Lines in Argon

Emissions of lines emanating from the 7s,6p,6s,5d,5p, 4d and 4p levels in argon were monitored during the active discharge and afterglow in three different gas mixtures. The gas mixtures studied were pure argon, 99% helium with 1% argon and a 50-50 mixture of helium and argon. Plots of photons accumulated vs. time are shown for several representative lines in figures 8 - 10 The relative intensities of each of the lines are tabulated in tables 1-3. Relative intensities are reported for the active discharge and 5 times during the afterglow. Transitions chosen for analysis are the 4p'(1/2)-4s'(1/2) transition at 7503 angstroms and the 5p'(1/2)-4s'(1/2) transition at 4259 angstoms. The 7503 angstrom line was chosen because the 4p' level lies well below the ground state of Ar_2^+ and is one of the levels of interest in the ^{3}He-Ar laser. The 4259 angstrom line was chosen because the 5p'

Figure 8. Plot of Intensity Versus Time at 7503 Angstroms.
Uncertainty is $\pm 0.14X(\text{Intensity})^{1/2}$

Symbols are: +-pure argon

x-1% argon

*-50% argon

The current pulse occurs at 20 μsec.

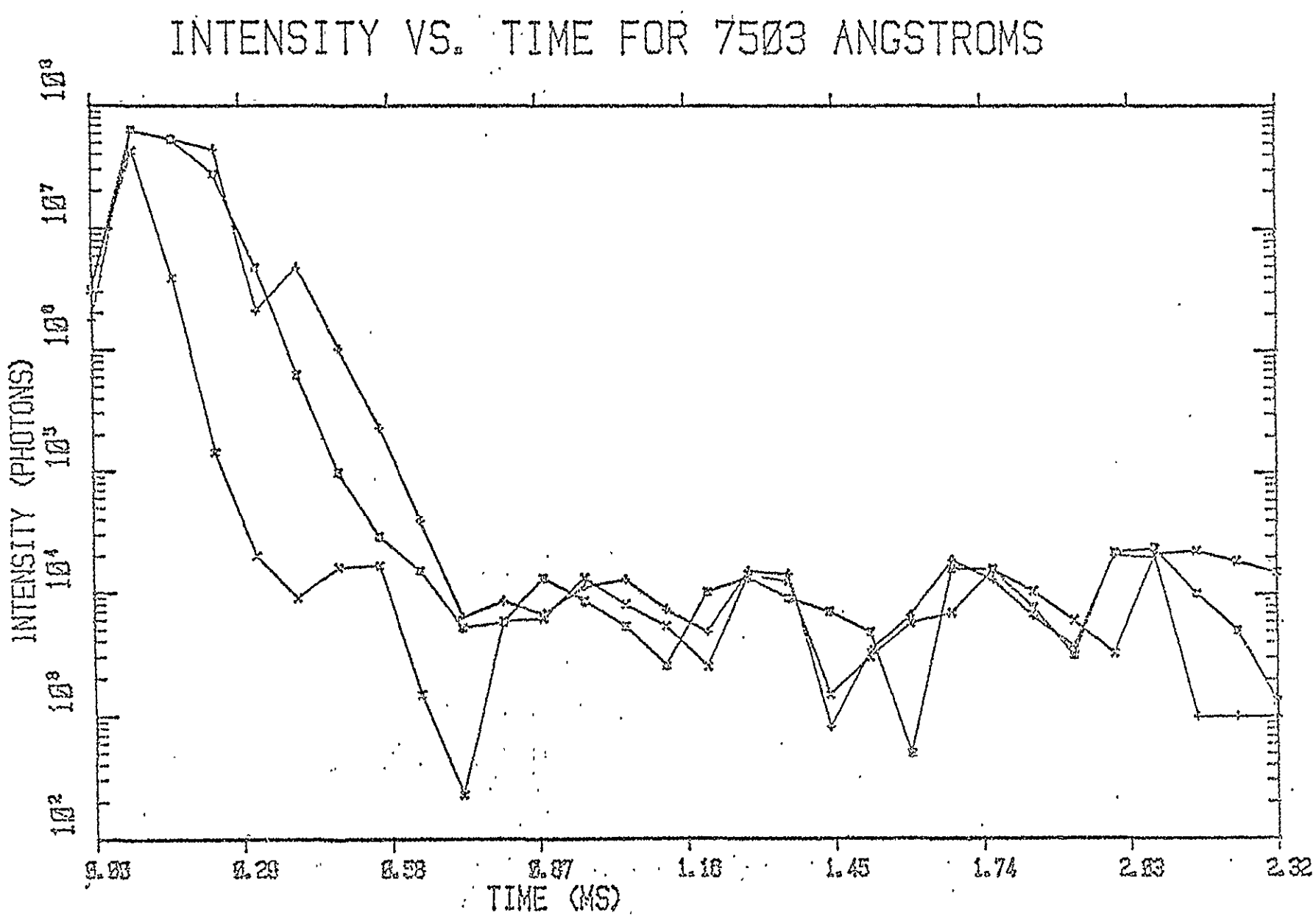
INTENSITY VS. TIME FOR 7503 ANGSTROMS
INTENSITY (PHOTONS)
10³
10⁷
10⁶
10⁵
10⁴
10³
10²
0.00
0.29
0.58
0.87
1.16
1.45
1.74
2.03
2.32
TIME (MS)

Figure 9. Plot of Intensity Versus Time for 5888 Angstroms.

Uncertainty is $\pm 0.14X(\text{Intensity})^{1/2}$.

Symbols are: +-pure argon

X-1% argon

*-50% argon

The current pulse occurs at 20 μsec.

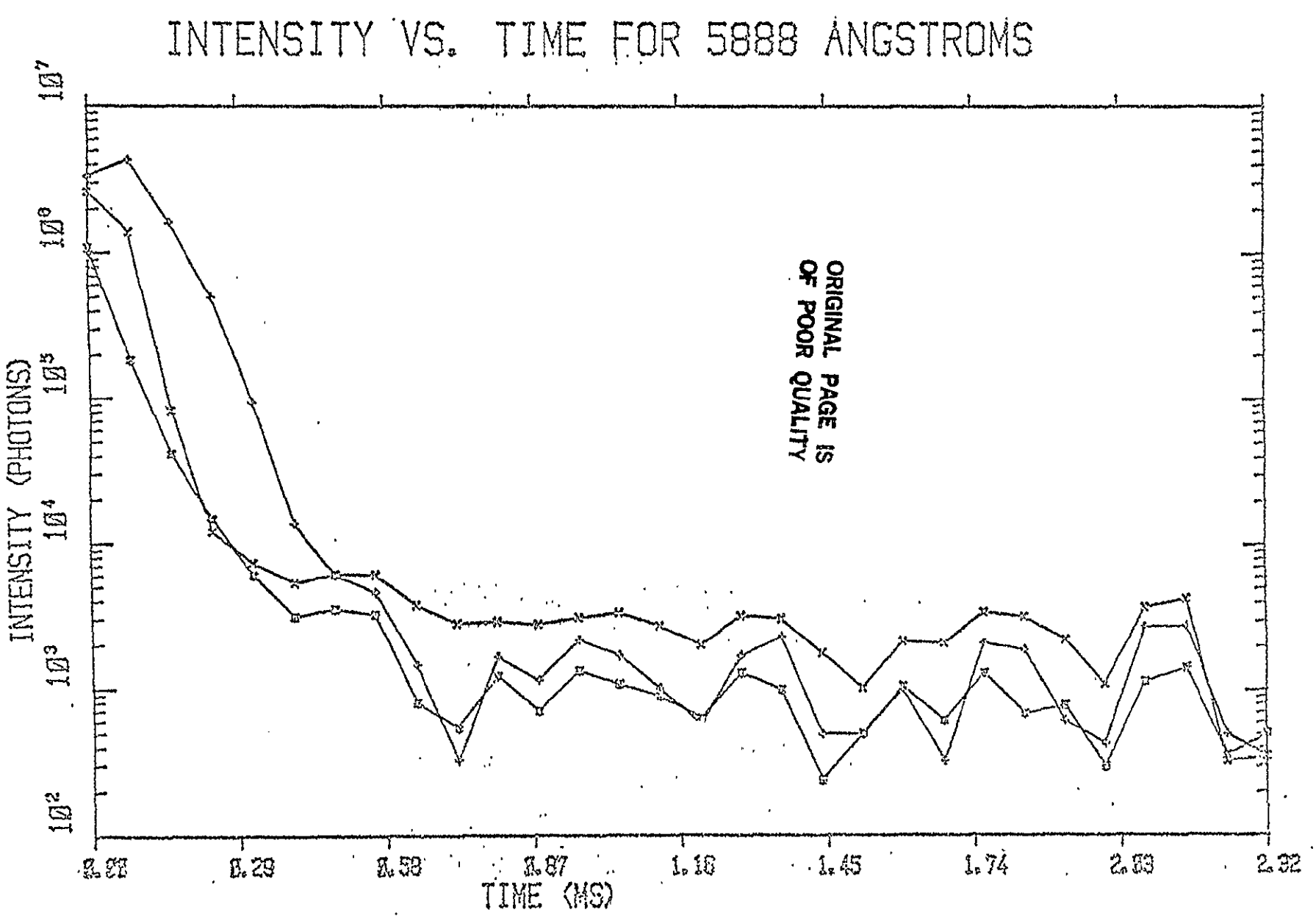
INTENSITY VS. TIME FOR 5888 ANGSTROMS
INTENSITY (PHOTONS)
10⁷
10⁶
10⁵
10⁴
10³
10²
0.00
0.29
0.58
0.87
1.16
1.45
1.74
2.03
2.32
TIME (MS)
ORIGINAL PAGE IS
OF POOR QUALITY

Figure 10. Plot of Intensity Versus Time for 4259 Angstroms.

Uncertainty is $\pm 0.14X(\text{Intensity})^{1/2}$

Symbols are: +-pure argon

X- 1% argon

*-50% argon

The current pulse occurs at 20 μsec.

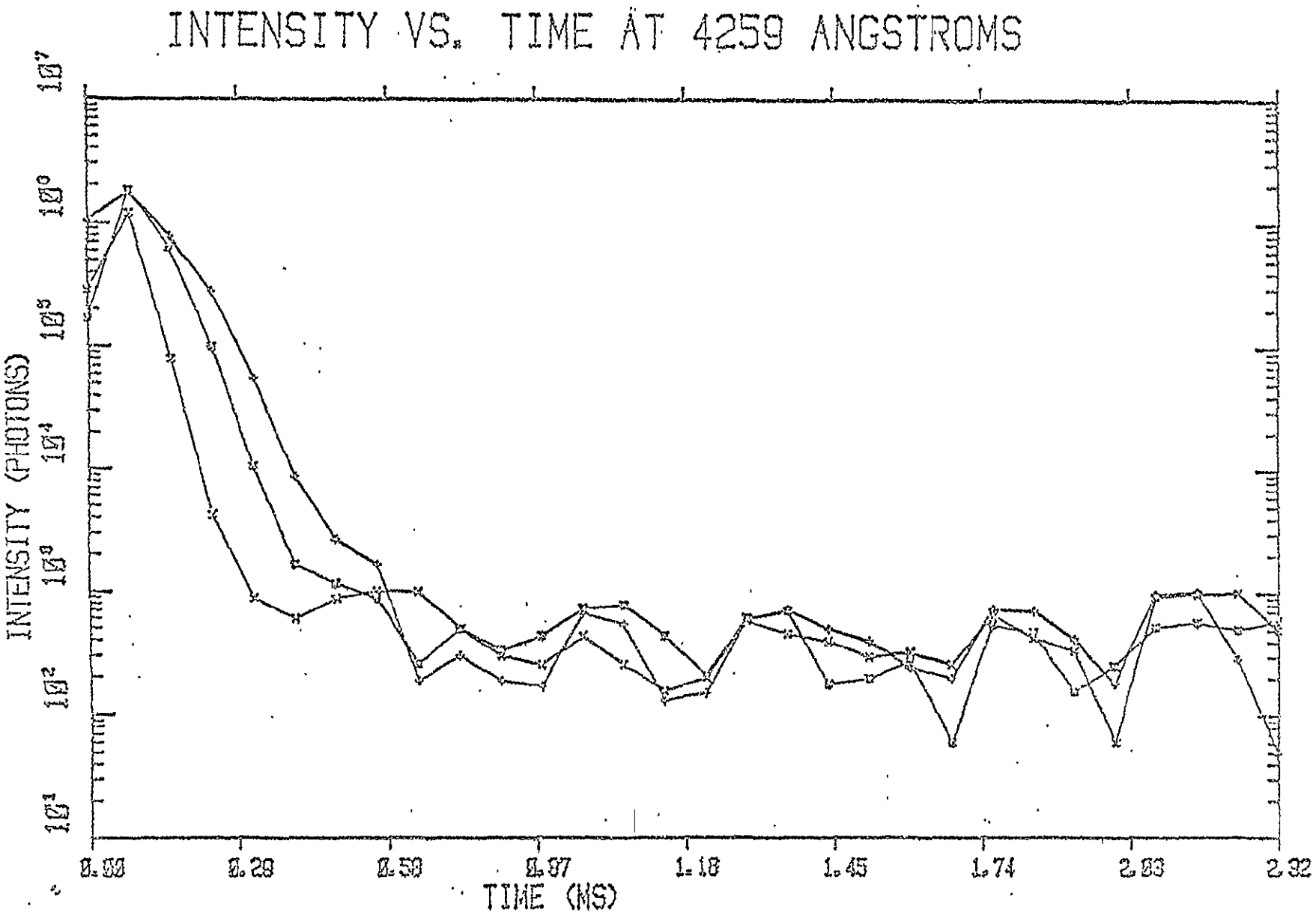
INTENSITY VS. TIME AT 4259 ANGSTROMS
INTENSITY (PHOTONS)
10⁷
10⁶
10⁵
10⁴
10³
10²
10¹
0.00
0.28
0.59
0.87
1.18
1.45
1.74
2.03
2.32
TIME (MS)

	Time after trigger (μsec)					
Wavelength (angstroms)	0	80	160	240	320	400
7503	23391	83147	71844	58626	2739	6268
7030	12352	28019	13232	3709	482	47
6937	3712	15929	6003	2386	761	188
5888	4431	5710	2386	662	123	18
5650	449	3869	761	395	97	17
4259	1382	2348	188	365	72	11
3649	698	93		11	3	1

Table 1. Relative Intensities in Pure Argon.
Trigger occurs 20 μsec before current pulse.

Wavelength (angstroms)	Time after trigger (μsec) 0	80	160	240	320	400
7503	12885	174545	15743	584	81	37
7030	42236	35455	2143	129	25	14
6937	6612	22857	1688	128	29	21
5888	10590	5570	333	49	30	22
5650	9156	3308	18	19	8	3
4250	1158	4887	321	17	4	2
3649	1630	100	10	3	2	1

Table 2. Relative Intensities in 99% Helium With 1% Argon. Trigger occurs 20 μsec before current pulse.

	Time after trigger (μsec)					
Wavelength (angstroms)	0	80	160	240	320	400
7503	17588	367639	308431	158741	27582	3535
7030	6719	120476	41412	4429	264	33
6937	10184	63237	4362	415	60	55
5888	6285	1057	241	86	35	18
5650	9637	1397	397	64	16	7
4259	982	10672	3713	574	61	10
3649	220	142	41	12	5	1

Table 3. Relative Intensities in 50% Helium with 50% Argon. Trigger occurs 20 μsec before current pulse.

level lies near the 3d level.

The evolution of the chosen transitions may be examined through the ratios of their emissions. The ratio of emission at 4259 angstroms to that at 7503 angstroms in pure argon falls off from 0.059 during the discharge to 0.028 50 μsec after the discharge and0.006 130 μsec after the discharge. A similar situation is encountered in the 1% and 50% mixtures. This is to be expected.

As the partial pressures of the gas mixtures are altered a marked effect is observed. The ratio of emission at 4259 angstroms to that at 7503 angstroms rises from 0.059 in pure argon to 0.090 in helim with 1% argon then falls off to 0.056 in the 50% mixture, during the active discharge. Early in the afterglow the ratio remains nearly constant as the partial pressures change but by 130 μsec into the afterglow the behavior is similar to that of the active discharge.

The high-pressure experiment yielded indeterminant results. Infrared radiation from an electron beam-generated plasma of pure argon at 300 Torr was scanned over the range of 1.5 μm to 1.84 μm. No signal was observed above the radio-frequency noise generated by the electron beam machine indicating that the sensitivity of the IR detection apparatus was insufficient.

Discussion

The plasma is assumed to be in a quasi-steady state, thus the intensity of emission from a given state, as expressed in number of photons is equal to the rate of population of

that state. In the model of Harries and Wilson dissociative recombination is assumed to be a population mechanism for the 4p level but not for the 5p level.[2] Collisional radiative recombination is assumed to be a population mechanism for both levels.

The collisional radiative recombination rate coefficient is typically expressed as the sum of a neutral part and an electronic part. In the low-pressure regime it may be assumed that the total rate coeffiecient is approximately equal to the electronic part. The collisional radiative rate coefficient is expressed as:

$$\alpha_{CRR}=A_{CRR}N_eT_e^{-x}$$

where A_{CRR} is a constant and x is unknown. The dissociative recombination rate coefficient is

$$\alpha_D=A_DT_e^{-.61}$$

Thus the ratio, R, of emission at 4259 angstroms to that at 7503 angstroms may be expressed as:

$$R=\frac{A_{CRR}N_eT_e^{-x}N_e\{Ar^+\}}{A_{CRR}N_eT_e^{-x}N_e\{Ar^+\}+A_DT_e^{-.61}N_e\{Ar_2^+\}}$$

The quasi-steady state assumption imposes the requirement that:

$$d\{Ar_2^+\}/dt=k\{He\}\{Ar\}\{Ar^+\}-A_DT_e^{-.61}N_e\{Ar_2^+\}=0$$

where $k\{He\}\{Ar\}\{Ar^+\}$ is the rate of formation of Ar_2^+. Or:

$$\{Ar^+\}=\frac{k\{He\}\{Ar\}\{Ar_2^+\}}{A_DT_e^{-.61}N_e}$$

Thus:

$$R=\frac{A_{CRR}T_e^{-x}N_e^2\{Ar^+\}}{A_{CRR}T_e^{-x}N_e^2\{Ar^+\}+k\{He\}\{Ar\}\{Ar^+\}}$$

$$R=\frac{1}{1+k\{He\}\{Ar\}/A_{CRR}T_e^{-x}N_e^2}$$

$$R\approx\frac{A_{CRR}T_e^{-x}N_e^2}{k\{He\}\{Ar\}}$$

In this expression k, A_{CRR}, {He} and {Ar} are constant with respect to time. Thus the ratio of the ratios at two different times during the afterglow may be written:

$$R_1/R_2=(N_{e1}/N_{e2})^2(T_{e1}/T_{e2})^{-x}$$

and:

$$-x=\ln\{(R_1/R_2)(N_{e2}/N_{e1})^2\}/\ln(T_{e1}/T_{e2})$$

The time evolution of electron density and electron temperature in a plasma under conditions similar to those in this study were measured by Monchicourt et. al.[8] Their results are shown in table 4 along with the other data pertinent to this discussion. The calculated values of -x are found to be 4.05 for pure argon, 0.255 for 1% argon and 6.43 for 50% argon.

Conclusions

Results of the high-pressure observations are inconclusive, indicating a need for further work in this area. The electron temperature dependences calculated from the results of the low-pressure observations, on the basis of the model of Harries and Wilson, are incompatible with generally accepted values. The model of Harries and Wilson and the results of this study are seen to be inconsistent with each other.

Time after discharge	50 μsec	130 μsec
R in pure argon	0.028	0.014
R in 99% He with 1% Ar	0.028	0.020
R in 50% He with 50% Ar	0.030	0.012
Electron Temperature[8]	780 K	710 K
Electron density[8]	9.0×10^{11} cm^{-3}	7.7×10^{11} cm^{-3}

Table 4. Parameters Used in Calculation of Temperature Dependence of Collisional Radiative Recombination Rate Coefficient.

APPENDIX I

ESTIMATIONS OF ELECTRON DENSITIES AND TEMPERATURES IN ^{3}HE-DOMINATED PLASMAS

by

B. D. DePaola, S. D. Marcum, H. K. Wrench, B. L. Whitten and W. E. Wells

ESTIMATIONS OF ELECTRON DENSITIES AND TEMPERATURES IN ^{3}He-DOMINATED PLASMAS*

by

B. D. De Paola, S. D. Marcum, H. K. Wrench, B. L. Whitten

and W. E. Wells

INTRODUCTION

It is well recognized that in order to make efficient use of the large energies derived from a fission reactor with a Nuclear Pumped Laser (NPL), a medium that will lase at high pressure must be employed. This is only one of the many features of future NPL's that will make them markedly different from common lasers of today. With this in mind we have made an attempt to characterize a high-pressure, ^{3}He-dominated NPL plasma, based on what is known of similar low pressure plasmas.

Many processes important to NPL's are strongly dependent upon electron temperature and/or electron density. Also, due to the nature of nuclear pumping, performing diagnostics on NPL plasmas is a very difficult, expensive and hazardous task. These facts provide the impetus for performing the calculations described here. These calculations are straightforward extrapolations of low pressure results into the high pressure regime. Several of the uncertainties inherent in this approach are also discussed.

THE PURE ^{3}He PLASMA

Taking helium as the sole species in the plasma, the following reactions were considered:

$$1)\quad S = \sigma \phi n_{(^3He)} \frac{\varepsilon_f}{W}$$

Equation 1 describes the production of He^+ where σ is the fission cross-section for ^{3}He, ϕ is the thermal neutron flux (assumed to be 10^{18} n-cm^{-2}-sec^{-1}), $n_{(^3He)}$ is the density of ^{3}He, ε_f is the energy released per fission of ^{3}He and W is the

energy invested per electron-ion pair produced (≈41.5eV).

2) $S_x = S/.56$.

This equation accounts for production of $He(2^3s)$ metastables which proceeds at roughly twice the rate of He^+ production.

3) $He^+ + 2He \longrightarrow He_2^+ + He$.

3-body conversion to He_2^+. This process varies as $78P_{He}^2$ (average of several measurements).

4) $He(2^3S) + He(2^3S) \longrightarrow He^+ + He + e$.

Metastable-metastable ionization which has the rate coefficient $\beta = 1.8 \times 10^{-9}$ cm^3-sec^{-1}.

5) $He(2^3S) + 2He \longrightarrow He_2(2^3\Sigma) + He$.

3-body conversion of metastables which scales as $.6P_{He}^2$.

6) $He_2^+ + e + X \Longrightarrow CRR$.

This represents collisional-radiative recombination which includes a very large number of possible processes.

7) $He(2^3S) + e \longrightarrow He + e$.

The last process considered is superelastic relaxation. The rate for this reaction is temperature dependent ($T_e^{1/2}$) and was derived from a detailed balancing calculation based on the forward process. (Reactions involving the helium singlet metastable were not considered because being only .8eV away from the $He(2^3S)$ state it is very quickly converted to the triplet metastable).

Using the above processes the following rate equations were developed:

$$\frac{d[He^+]}{dt} = S + 1/2\ \beta\ [He(2^3S)] - 78\ P_{He}\ [He^+]$$

Here the first source term is due to ionization by high energy electrons produced by the fission products of ^3He; the second is due to metastable-metastable ionization. The loss term is due to 3-body conversion. For He_2^+ we have

$$\frac{d[He_2^+]}{dt} = .78\ P_{He}\ [He^+] - \alpha\ [He_2^+]\ n_e, \text{ where}$$

$$\alpha = 4.5 \times 10^{-20}(T_e/T_o)^{-4\pm.5} n_e + 5 \times 10^{-27}(T_e/T_o)^{-1\pm1} n_o;\ T_e,\ T_o,\ ne,\ no$$

are electron and gas temperatures and the electron and neutral densities, respectively. The source term is due to 3-body conversion whereas the loss is due to collisional-radiative recombination. Note the electron temperature and density dependencies. For helium metastables the rate equation is

$$\frac{d[He(2^3S)]}{dt} = S_x + .7\,\alpha\,[He_2^+]\,n_e - \beta\,[He(2^3S)]^2 - \gamma\,[He(2^3S)]\,n_e - .6\,P_{He}^2\,[He(2^3S)]$$

where $\gamma = 7 \times 10^{-11}\,T_e^{1/2}$. The source terms here are due to excitation by high energy electrons produced by the fission products of ^3He and collisional-radiative recombination of He_2^+. Losses are due to metastable-metastable ionization, superelastic relaxation and 3-body conversion of metastables, respectively. For electron density we have

$$\frac{d\,n_e}{dt} = S + 1/2\,\beta\,[He(2^3S)]^2 - \alpha\,[He_2^+]\,n_e.$$

Here, of course, we have the same source terms as with He^+; the loss is assumed to be due to collisional-radiative recombination. Also considered was the following energy balance equation:

$$\frac{d(3/2\,nkT)}{dt} = S\,\Delta\varepsilon_{e-e} + 1/2\,\beta\,[He(2^3S)]^2\,\Delta\varepsilon'_{e-e} + \gamma\,n_e\,[He(2^3S)]\,\Delta\varepsilon''_{e-e} - \frac{2m}{M}(3/2\,k)\,(T_e - T_o)\,\nu_{eo}$$

The source terms are due to ionization by high energy electrons produced by the ^3He fission products, metastable-metastable ionization and superelastic relaxation. $\Delta\varepsilon_{e-e}$, $\Delta\varepsilon'_{e-e}$, and $\Delta\varepsilon''_{e-e}$ are defined as the energies transferred to the maxwellian part of the electron energy distribution by a non-maxwellian electron at 10, 15 and 20 eV respectively. The loss term is due to electron-neutral collisions with ν_{eo} being the electron-neutral collision frequency.

We have an electron energy distribution like that of Figure 1. High energy electrons produced in REGION III by the ^3He fission products cascade down in energy toward a primarily maxwellian region of the distribution (REGION I).

Beyond the first excitation potential of He, inelastic collisions dominate. At and below the first excitation potential of helium production of He^+ and $He(2^3S)$ occurs. Wells et. al. have shown that the energy transferred to the maxwellian part of the electron energy distribution by a non-maxwellian electron is a function of electron density and pressure (Figure 2). All values of $\Delta\varepsilon$ used in this calculation were extrapolated from the work of Wells.

Using the above rate equations in steady-state form we calculated electron temperature and density as a function of pressure from 100 to 2300 torr. With these temperatures and densitites we were also able to calculate the densities of He^+, He_2^+ and the density of the $He(2^3S)$ metastable, all as functions of pressure. However, pure helium is not expected to make a very good lasing medium, so we next considered a mixture of helium and argon. Results for the pure helium plasma will be shown later in comparison to those for the helium-argon mixture.

THE He-Ar (1%Ar) PLASMA

Upon adding 1% argon to the plasma, all reactions considered earlier with helium alone are still operative. However, several other reactions with argon must now be taken into account. In Figure 3, equations 1-7 are for a pure helium plasma. Equations 8-15 include possible He-Ar reactions as well as Ar-Ar reactions. Eq. 8 - charge exchange with He^+; 9- charge exchange with He_2^+; 10 - 3-body charge exchange; 11 - Penning ionization of argon; 12 - dissociative recombination; 13 - 3 body conversion; 14 - collisional-radiative recombination; and 15 - associative ionization to Ar_2^+. In the case of collisional-radiative recombination we assumed this reaction to be identical to collisional-radiative recombination of He.

The rate equations listed earlier must now be modified to include these reactions. Figure 4 lists the updated set of rate equations; additions to the

rate equations for the pure helium plasma are underlined. For example, He^+ can now be lost through charge exchange with Ar. He_2^+ can also be lost through charge exchange as well as 3-body conversion, etc. However, considering steady state conditions, those equations can be solved for electron temperature and density as functions of pressure, as well as the densities of all other species in the plasma.

RESULTS

Figure 5 is a plot that compares electron temperature with and without argon. Both are plotted against pressure from 100 to 2300 torr. Note that the electron temperature is over 1000K at low pressures, but tends toward room temperature at higher pressures. This is important because of the dependence of the various coefficients on electron temperature. Also note that the addition of 1% Ar to the plasma does not significantly affect the electron temperature.

Figure 6 compares electron densities with and without argon. Here the variation in electron denisty with pressure is not so great as was the temperature change, but again note the dependence of the rate coefficients on electron density. Figure 7 is a plot of He^+ density versus pressure with 0% and 1% Ar. Upon adding argon to the plasma the He^+ density is lower at all pressures. This is reasonable considering that charge exchange between He^+ and Ar can now occur. Similarly, Figure 8 shows He_2^+ density with and without argon plotted against pressure. The large decrease in He_2^+ concentration at all pressures is due to 2- and 3-body charge exchange with argon. Figure 9 plots the helium metastable ($He(2^3S)$) density versus pressure also with and without argon. The decrease in the helium metastable density with 1% Ar at all pressures is due to Penning ionization of argon. Also, densities of Ar^+, Ar_2^+, and Ar were calculated as functions of pressure and are shown in Figure 10. The argon excited state density represents an accumulation of all argon excited states that exist between the ionization limits of the atomic

and molecular ions into a single state. This was done so that associative ionization of argon could be considered.

CONCLUSIONS

The above results are reasonable based on extrapolation of the knowledge of low-pressure ^{3}He-dominated plasmas. However:

1. What is the collisional-radiative recombination rate coefficient at high pressures? We have employed a low presssure coefficient in our calculations that may or may not be valid at higher pressures.

2. We have assumed that recombination of Ar^+ is in the collisional radiative form, which seems reasonable, but we've assumed collisional radiative recombination of argon to be identical to that of helium. This later assumption may well be a dubious one.

3. What other processes are important at higher pressures that we could not consider? It is possible that He_3^+, Ar_3^+ and/or $HeAr^+$ achieve large densities at higher pressures such that they become important species in the plasmas. These could not be considered in our analysis.

These are examples of the questions that this type of calculation raises. While it is true that there are more sophisticated methods of calculating electron temperatures and densities, given the uncertainties in cross sections and other data we feel that the approach outlined here is sufficient for the present.

*This research was sponsored in part by the National Aeronautics and Space Administration.

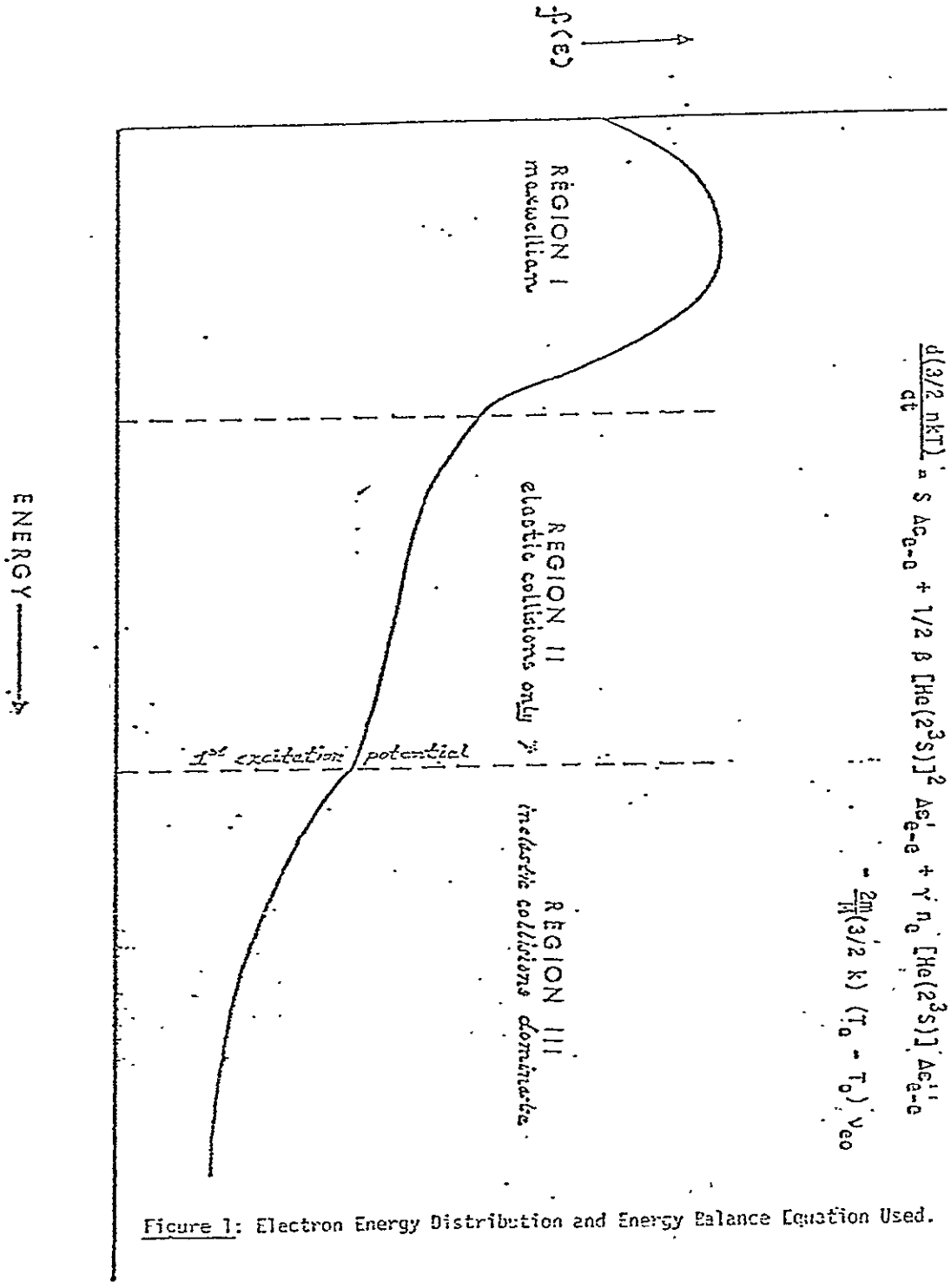

Figure 1: Electron Energy Distribution and Energy Balance Equation Used.

Heating of a maxwellian distribution due to a non maxwellian electron

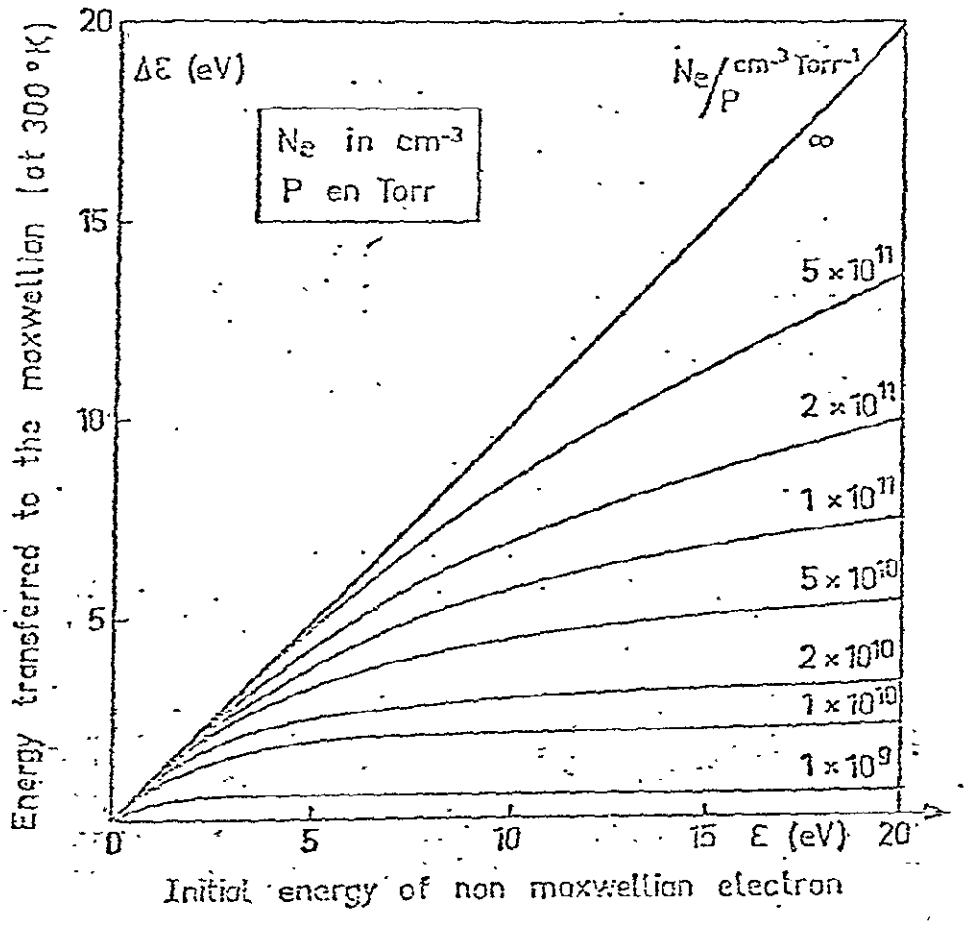

Figure 2:

REACTIONS CONSIDERED

1.	$S = \sigma \phi n_{(^3He)} \frac{\varepsilon_f}{W}$ (He$^+$ source)	
2.	$S_x = S/.55$ (He(2^3S) source)	
3.	$He^+ + 2He \longrightarrow He_2^+ + He$	$\propto 78P_{He}^2$
4.	$He(2^3S) + He(2^3S) \longrightarrow He^+ + He + e$	$\beta = 1.8 \times 10^{-9}$ cm^3-sec^{-1}
5.	$He(2^3S) + 2He \longrightarrow He_2(2^3\Sigma) + He$	$\propto .6P_{He}^2$
6.	$He_2^+ + e + X \Longrightarrow$ CRR	
7.	$He(2^3S) + e \longrightarrow He + e$	$7 \times 10^{-11} T_e^{1/2}$

OTHER REACTIONS WITH ARGON (1%)

8.	$He^+ + Ar \longrightarrow Ar^+ + He$	$\sigma = 10^{-17}$ cm^2
9.	$He_2^+ + Ar \longrightarrow Ar^+ + 2He$	$\beta_1 = 2.2 \times 10^{-10}$ cm^3-sec^{-1}
10.	$He_2^+ + Ar + He \longrightarrow Ar^+ + 3He$	$\gamma_1 = 2.4 \times 10^{-29}$ cm^6-sec^{-2}
11.	$He(2^3S) + Ar \longrightarrow Ar^+ + He + e$	$\beta_3 = 7 \times 10^{-16}$ cm^2
12.	$Ar_2^+ + e \longrightarrow Ar^* + Ar$	$\alpha_D = 9.1 \times 10^{-7} (300/T_e)^{.67}$ cm^3-sec^{-1}
13.	$Ar^+ + Ar + He \longrightarrow Ar_2^+ + He$	$\propto 376P_{He}P_{Ar}$
14.	$Ar^+ + e + X \Longrightarrow$ CRR	
15.	$Ar^* + Ar \longrightarrow Ar_2^+$	2×10^{-9} cm^3-sec^{-1}

Figure 3: Reactions Considered in this Study.

RATE EQUATIONS

$$\frac{d[He^+]}{dt} = S + 1/2\ \beta\ [He(2^3S)] - 78\ P_{He}\ [He^+] - \sigma\langle v\rangle\ [He^+]\ [Ar]$$

$$\frac{d[He_2^+]}{dt} = 78\ P_{He}\ [He^+] - \alpha\ [He_2^+]\ n_e - \beta_1\ [He_2^+]\ [Ar] - \gamma_1\ [He_2^+]\ [Ar]\ [He]$$

$$\frac{d[He(2^3S)]}{dt} = S_x + .7\ \alpha\ [He_2^+]\ n_e - \beta\ [He(2^3S)]^2 - \gamma\ [He(2^3S)]\ n_e - .6\ P_{He}^2\ [He(2^3S)] - \beta_3\ [Ar]\ [He(2^3S)]$$

$$\frac{d\ n_e}{dt} = S + 1/2\ \beta\ [He(2^3S)]^2 - \alpha\ [He_2^+]\ n_e + \beta_3\ [Ar]\ [He(2^3S)] - \alpha_0\ [Ar_2^+]\ n_e - \alpha\ [Ar^+]\ n_e + 2 \times 10^{-9}\ [Ar^*]\ [Ar]$$

$$\frac{d[Ar^+]}{dt} = \sigma\langle v\rangle\ [He^+]\ [Ar] + \beta_1\ [He_2^+]\ [Ar] + \gamma_1\ [He_2^+]\ [Ar]\ [He] + \beta_3\ [He(2^3S)]\ [Ar] - 376\ P_{He}\ P_{Ar}\ [Ar^+] - \alpha\ [Ar^+]\ n_e$$

$$\frac{d[Ar_2^+]}{dt} = 2 \times 10^{-9}\ [Ar^*]\ [Ar] + 376\ P_{He}\ P_{Ar}\ [Ar^+] - \alpha_0\ [Ar_2^+]\ n_e$$

$$\frac{d[Ar^*]}{dt} = \alpha\ [Ar^+]\ n_e - 2 \times 10^{-9}\ [Ar^*]\ [Ar] - [Ar^*]/\alpha\ n_e$$

Where:

$$S = \sigma\ \phi\ n_{(^3He)}\ \frac{\epsilon_f}{W}$$

$$S_x = S/.55$$

$$\gamma = 7 \times 10^{-11}\ T_e^{1/2}$$

$$\alpha = 4.5 \times 10^{-20}\ (T_e/T_o)^{-4\pm.5} n_e + 5 \times 10^{-27} (T_e/T_o)^{-1\pm1} n_o$$

$$\sigma\langle v\rangle = 6 \times 10^{-13} \qquad \beta_3 = 4.2 \times 10^{-11}$$

$$\beta_1 = 2.2 \times 10^{-10} \qquad \alpha_0 = 9.1 \times 10^{-7}\ (T_e/T_o)^{-.67}$$

$$\gamma_1 = 2.4 \times 10^{-24}$$

Figure 4: Rate Equations Employed in this Study.

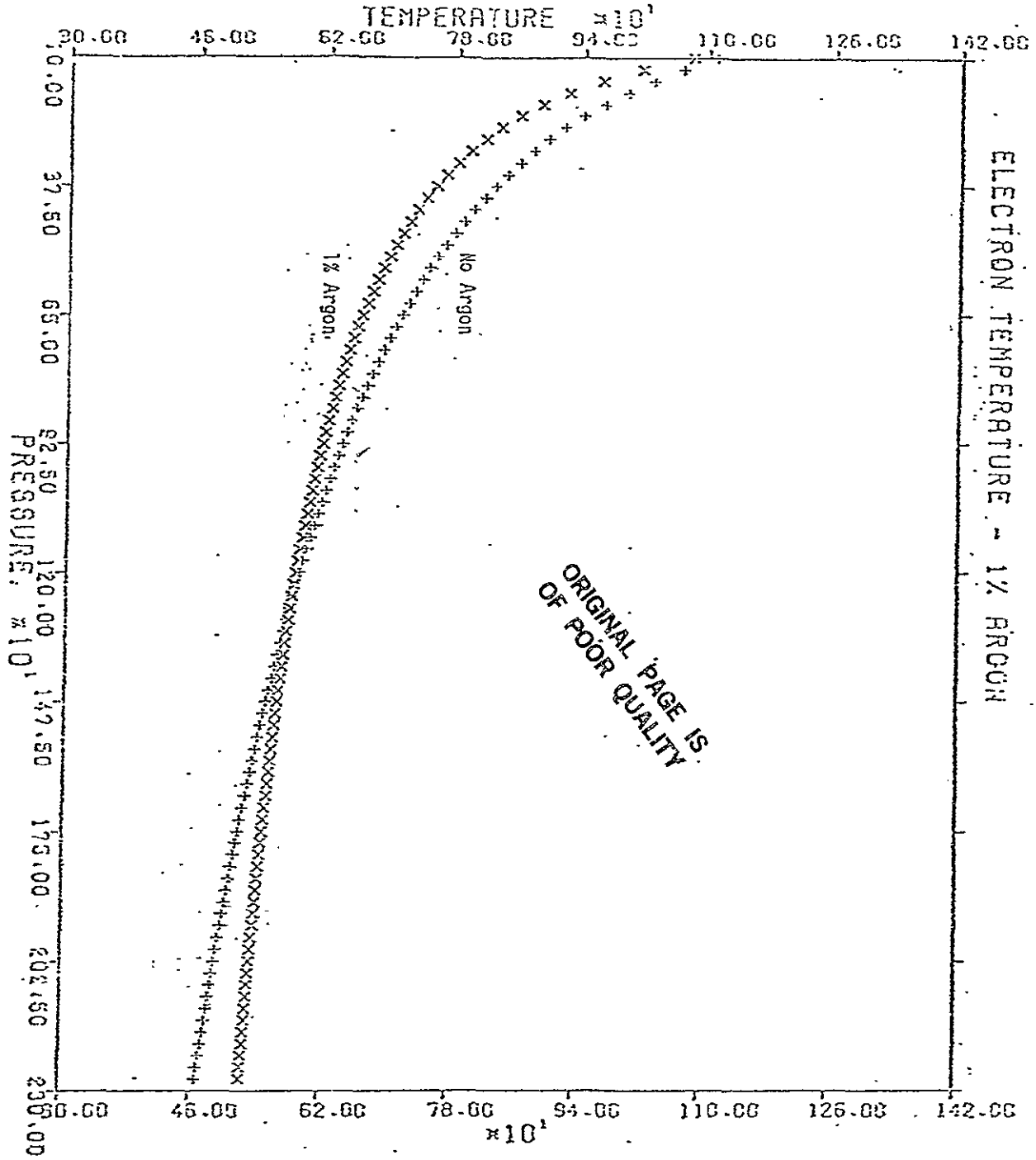

Figure 5: Plot of Electron Temperature versus Pressure.

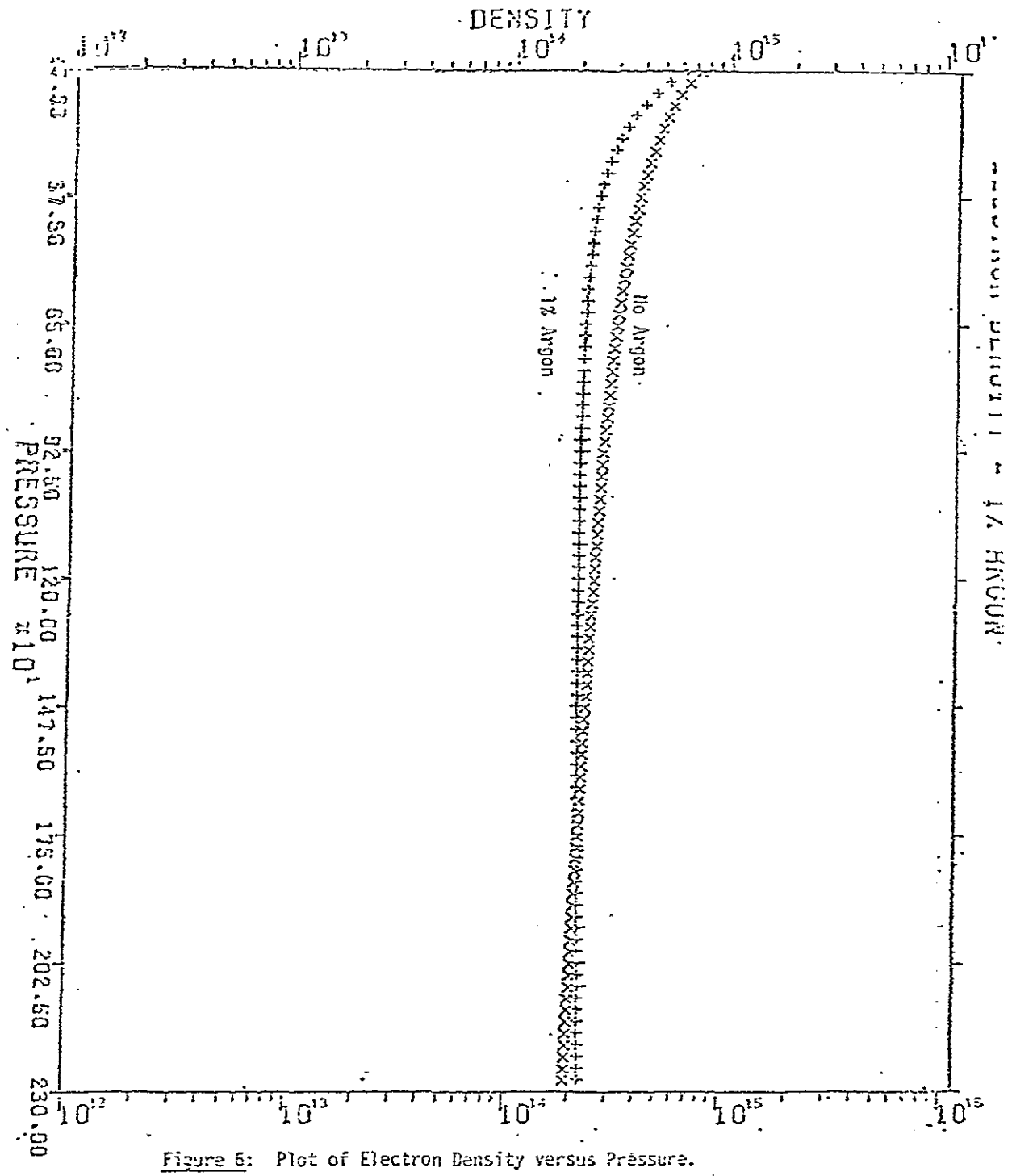

Figure 6: Plot of Electron Density versus Pressure.

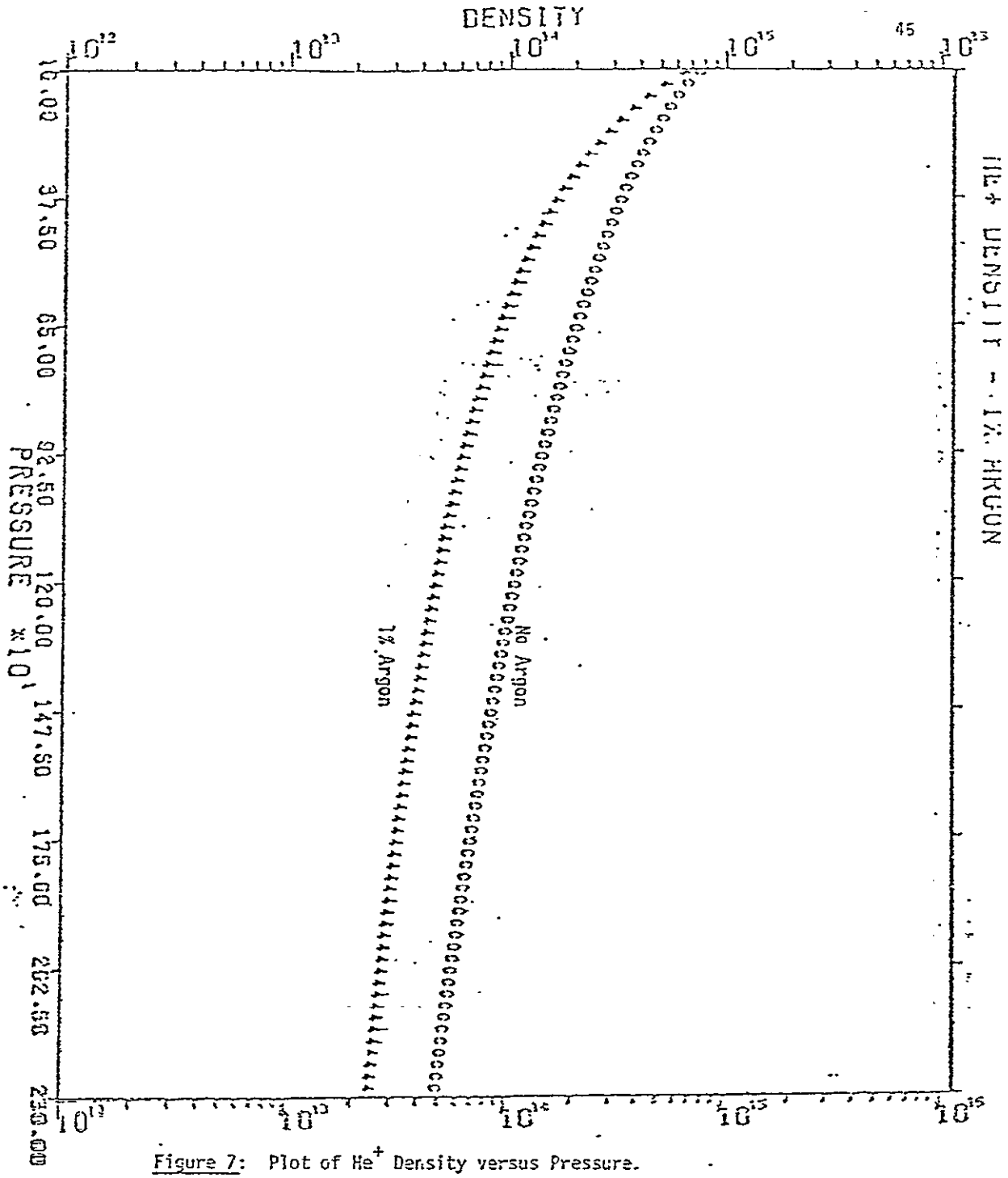

Figure 7: Plot of He^{+} Density versus Pressure.

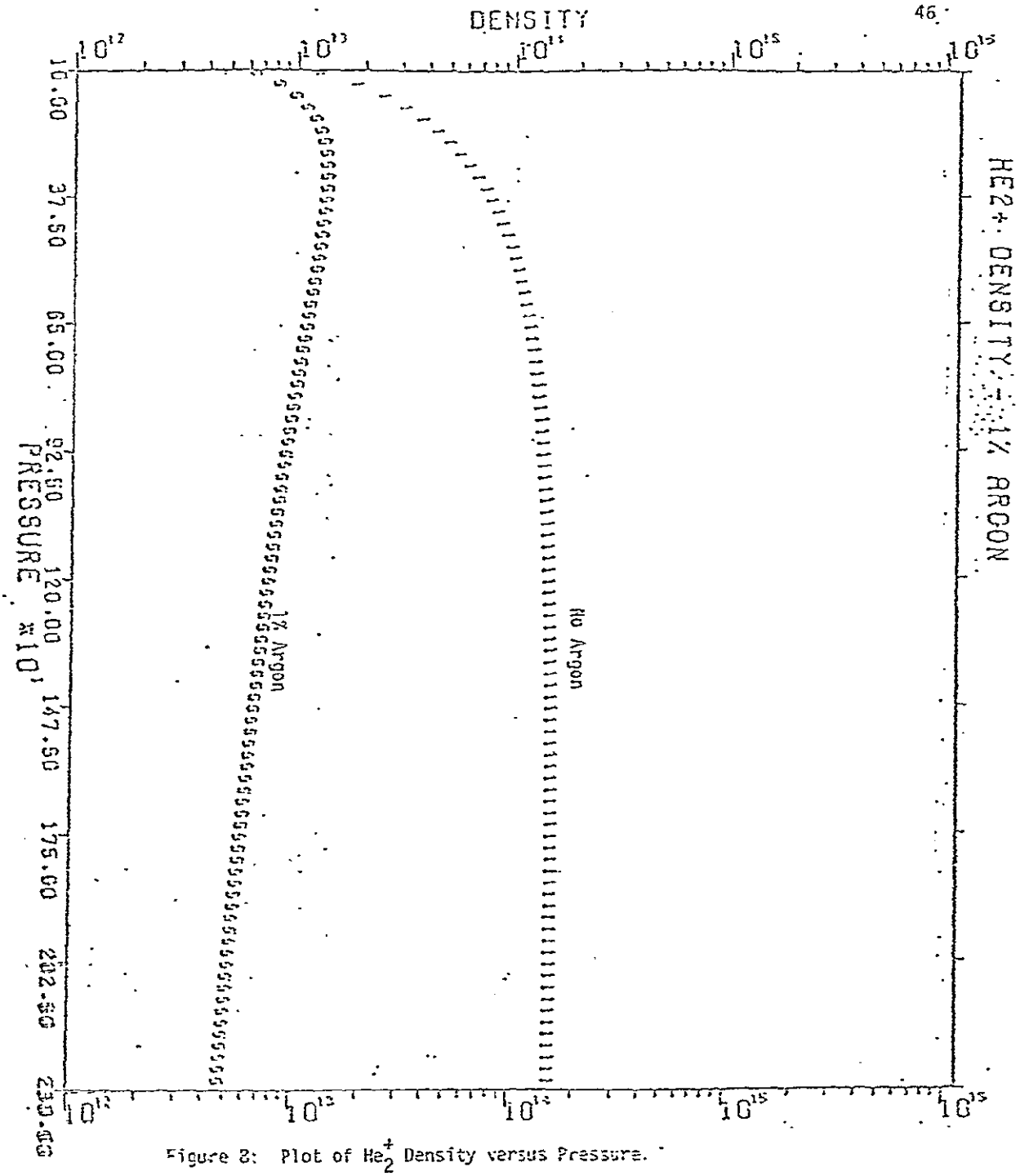

Figure 8: Plot of He_2^+ Density versus Pressure.

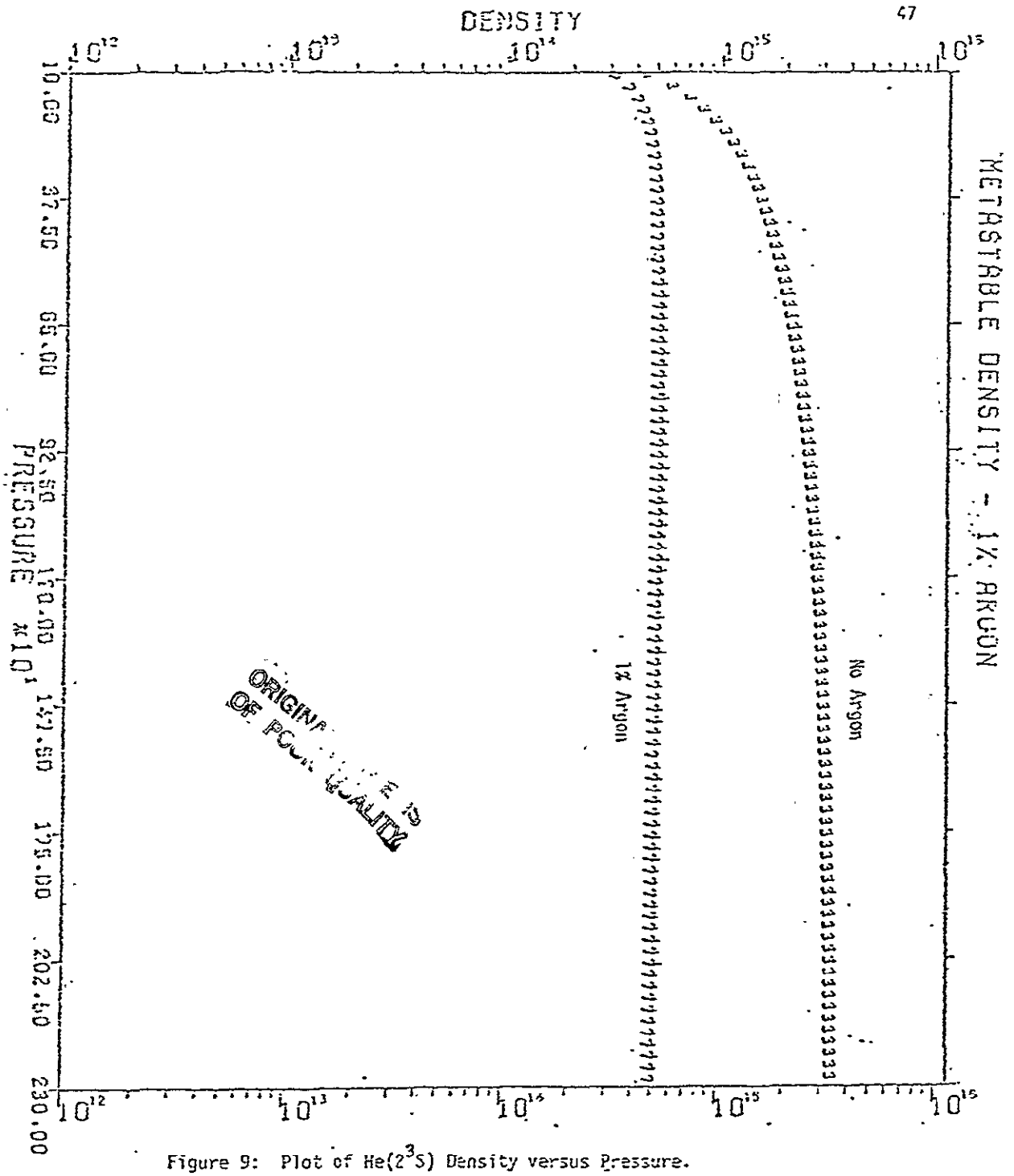

Figure 9: Plot of He(2^3S) Density versus Pressure.

APPENDIX II

Program to Calculate Electron Densities and Temperatures

```
C     THIS PROGRAM SOLVES A SYSTEM OF NONLINEAR EQUATIONS BY
C SUCCESSIVE ITERATIONS.  A SYSTEM OF SEVEN SIMULTANEOUS
C EQUATIONS HAS BEEN REDUCED ANALYTICALLY TO TWO NONLINEAR,
C SIMULTANEOUS EQUATIONS IN ELECTRON DENSITY AND ELECTRON
C TEMPERATURE.  IN EACH ITERATION STEP THE SSP SUBROUTINE
C RTMI, SUPPLIED BY IBM IS USED TO SOLVE A NONLINEAR EQUATION.
C THE SUBROUTINE RTMI SOLVES FOR A ROOT OF AN EXTERNAL FUNCTION
C SET EQUAL TO ZERO.
      COMMON DE(3),XNEO,TEO,XAB(3),PH,PA,P,V,SIG13,FLX,FF,SIG1,B11,B2,GA
     -M,SIG4
      REAL YZ(610,9)
      EXTERNAL FCT
      EXTERNAL FCN
C     FORMAT PRINTED OUTPUT
  500 FORMAT(' ',3X,'P(HE)=',E14.7,3X,'P(AR)=',E14.7,3X,'P(TOTAL)=',E14.
     -7)
  550 FORMAT (' METASTABLE DENSITY = ', E 14.7)
  570 FORMAT (' ELECTRON DENSITY = ', E14.7)
  590 FORMAT(' ','ELECTRON TEMPERATURE=',E14.7)
  610 FORMAT(' AR2=',E14.7)
  611 FORMAT(' AR=',E14.7)
  612 FORMAT(' RECOMBINATION=',E14.7)
  613 FORMAT(' HE2=',E14.7)
  614 FORMAT(' HE=',E14.7)
  620 FORMAT(' ','***** NO CONVERGENCE *****')
  640 FORMAT(' ',' GARBAGE  GARBAGE  GARBAGE  GARBAGE')
  670 FORMAT('1')
  680 FORMAT ('0')
C     DEFINE PARAMETERS AND INITIALIZE VARIABLES
      N2=1
      N=2
      XNEO=1.0E12
      TEO=305.
      PH=1504.8
      X=.01
      PA=X*PH
      P=PA+PH
      PAI=PA
      PHI=PH
      PI=P
      V=6.0E4
      SIG13=5.0E-21
      FLX=1.E17
      FF=2.3E4
      SIG1=1E-17
      B11=1.8E-9
      B2=2.2E-10
      GAM=2.4E-29
      SIG4=7.0E-16
C     THE FOLLOWING SOLVES AN ENERGY PARTITION EQUATION FOR THE
C ENERGY TRANSFERRED TO THE NEAR-MAXWELLIAN PART OF A NON-
C MAXWELLIAN ELECTRON ENERGY DISTRIBUTION FUNCTION
  200 AA=6.93E-5*XNEO
      P=PH+PA
```

```
      BB=1.34E-11*3.55E19*P
      CC=2.36E-11*3.55E19*P
      AAA=SQRT(AA/BB)
      XK = (AA/CC)**(1./3.)
      ABC=AAA*(ATAN(3/AAA)-ATAN(1.29E-4*TEO/AAA))
      ABB=.67*(XK**2)*((.5*ALOG(1-(3*XK*1.73/((XK+1.73)**2))))+(1.73*ATA
     -N((3.46-XK)/(1.73*XK))))
      M=0
      NN=0
  280 DO 295 N=10,20,5
      NN=0
      NN=NN+1
      IF(1-(3*XK*SQRT(FLOAT(N))/(XK+SQRT(FLOAT(N))**2)))290,290,285
  285 XAB(NN)=.67*(XK**2)*(.5*ALOG(1-(3*XK*SQRT(FLOAT(N))/(XK+SQRT(FLOAT
     T(N))**2)))+(1.73*ATAN(((2*SQRT(FLOAT(N)))-XK)/(XK*1.73))))
      M=M+1
      DE(M)=ABC+XAB(NN)-ABB
      IFLAG=0
      GO TO 295
  290 M=M+1
      DE(M)=ABC
      IFLAG=1
  295 CONTINUE
C    CALCULATE ELECTRON TEMPERATURE
      S=FCT(TEO)
      IF (S) 1011,1012,1013
C     CALL SUBROUTINE TO SEARCH FOR RIGHT-HAND BOUNDARY USED IN RTMI
 1011 CALL TPOS(S,S1,XRI,XLI)
      GO TO 36
 1012 TEN=TEO
      GO TO 37
C     CALL SUBROUTINE TO SEARCH FOR LEFT-HAND BOUNDARY USED IN RTMI
 1013 CALL TNEG(S,S1,XRI,XLI)
C     CALL SUBROUTINE TO SOLVE ENERGY BALANCE EQUATION
   36 CALL RTMI(TEN,F,FCT,XLI,XRI,1.,1000,IER)
      FN=F
      IERN=IER
      IF (IER-2)37,1999,37
C     CHECK CONVERGENCE OF ENERGY BALANCE EQUATION
   37 IF((ABS(TEO-TEN)/TEO)-0.0001)710,710,700
  700 TEO=TEN
      GO TO 200
C    CALCULATE ELECTRON DENSITY
  710 S=FCN(XNEO)
      IF(S)1001,1002,1003
C     CALL SUBROUTINE TO SEARCH FOR RIGHT-HAND BOUNDARY USED IN RTMI
 1001 CALL NPOS(S,S1,XRI,XLI)
      GO TO 56
 1002 XNEN=XNEO
      GO TO 57
C     CALL SUBROUTINE TO SEARCH FOR LEFT-HAND BOUNDARY USED IN RTMI
 1003 CALL NNEG(S,S1,XRI,XLI)
C     CALL SUBROUTINE TO SOLVE ELECTRON DENSITY CONTINUITY EQUATION
   56 CALL RTMI(XNEN,F,FCN,XLI,XRI,1.,1000,IER)
```

```
      IF (IERN-2)57,1999,57
C     CHECK CONVERGENCE OF ELECTRON DENSITY CONTINUITY EQUATION
   57 IF((ABS(XNEO-XNEN)/XNEO)-0.0001)465,465,460
  460 XNEO=XNEN
      GO TO 200
 1999 WRITE(6,620)
  465 IF (IFLAG)480,480,470
  470 WRITE(6,640)
C     CALCULATE ION AND METASTABLE DENSITIES FROM SOLUTIONS FOR
C ELECTRON TEMPERATURE AND ELECTRON DENSITY
  480 ALF9=4.0E-20*(300./TEN)**4*XNEN+1.8E-10*(300./TEN)*P
      ALFD=9.1E-7*(300./TEN)**.61
      ALF12=7.0E-11*SQRT(TEN)
      C1=SIG13*FLX*3.55E16*PH*FF/(78.*PH**2+SIG1*V*3.55E16*PA)
      C2=.5*B11/(78.*PH**2+SIG1*V*3.55E16*PA)
      C3=78*PH**2/(B2*3.55E16*PA+GAM*1.26025E33*PA*PH+ALF9*XNEN)
      C4=(SIG1*V*3.55E16*PA+(B2+GAM*3.55E16*PH)*3.55E16*PA*C3)/(ALF9*XNE
     -N+376.*PH*PA)
      C5=SIG4*V*3.55E16*PA/(ALF9*XNEN+376.*PA*PH)
      AA10=B11-(27.3*ALF9*PH*PH*B11*XNEN/(78*PH*PH+3.55E-1*V*PA)/(ALF9*X
     -NEN+2.2E-10*3.55E16*PA+2.4E-29*1.26025E33*PH*PA))
      BB10=1.491E6*PA+ALF12*XNEN+.6*PH*PH
      CC10=-SIG13*FLX*3.55E16*PH*FF/.56-(54.6*ALF9*PH*PH*SIG13*FLX*3.55E
     -16*PH*FF*XNEN/(78*PH*PH+3.55E-1*V*PA)/(ALF9*XNEN+2.2E-10*3.55E16*P
     -A+2.4E-29*1.26025E33*PA*PH))
      C10=(-BB10+SQRT(BB10**2-4*AA10*CC10))/2/AA10
  490 HE=C1+C2*C10*C10
      HE2=C3*HE
      AR=C4*HE+C5*C10
      FINIS=ALF9*AR*XNEN/(2.E-9*3.55E16*PA+(    (ALF9*XNEN)))
      AR2=(2E-9*FINIS*3.55E16*PA+376.*PH*PA*AR)/(ALFD*XNEN)
      XNE=AR+AR2+HE+HE2
      IF(ABS(XNE-XNEN)/XNEN-.01  )15,15,10
   10 PH=PH1-(HE+HE2)/3.55E16
      PA=PA1-(AR+AR2)/3.55E16
      XNE=XNEN
      GO TO 200
C     PRINT RESULTS
   15 WRITE(6,680)
      WRITE(6,500)PH1,PA1,P1
      WRITE(6,550)C10
      WRITE(6,570)XNEN
      WRITE(6,590)TEN
      WRITE(6,611) AR
      WRITE(6,610) AR2
      WRITE(6,613)HE2
      WRITE(6,614)HE
      WRITE(6,570)XNE
      STOP
      END

      SUBROUTINE TPOS(S,S1,XRI,XLI)
C     THIS SUBROUTINE SEARCHES FOR THE RIGHT-HAND BOUNDARY USED
```

```
C BY RTMI IN SOLVING THE ENERGY BALANCE EQUQTION.
C      THE SEARCH IS PERFORMED BY INCREMENTING THE ARGUMENT OF
C THE EXTERNAL FUNCTION FCT IN THE DIRECTION OF INCREASING VALUE
C OF THE FUNCTION UNTIL A POSITIVE VALUE IS ENCOUNTERED.  CONTROL
C IS THEN RETURNED TO THE MAIN PROGRAM.
      COMMON DE(3),XNEO,TEO,XAB(3),PH,PA,P,V,SIG13,FLX,FF,SIG1,B11,B2,GA
     -N,SIG4
      I1=0
      J1=0
      TE=1.01*TEO
      TE1=TEO
      S=FCT(TEO)
      S1=FCT(TE)
      IF (S1)1004,1004,1028
1004  IF (S-S1)1007,1005,1005
 997  TE1=TEO
1005  TE=TE1/1.01
      S=FCT(TE)
      IF(S)1001,1001,1028
1001  I1=I1+1
      IF (I1-800)1006,1006,1003
 1003 IF (J1-800)999,999,1028
1006  TE1=TE
      GO TO 1005
 999  TE1=TEO
 1007 TE=TE1*1.01
      S=FCT(TE)
      IF(S)1002,1002,1028
1002  J1=J1+1
      IF(J1-800)1008,1008,1009
 1009 IF (I1-800)997,997,1028
1008  TE1=TE
      GO TO 1007
1028  XRI=TE
      XLI=TEO
      RETURN
      END

      SUBROUTINE TNEG(S,S1,XRI,XLI)
C     THIS SUBROUTINE SEARCHES FOR THE LEFT-HAND BOUNDARY USED
C BY RTMI IN SOLVING THE ENERGY BALANCE EQUQTION.
C     THE SEARCH IS PERFORMED BY INCREMENTING THE ARGUMENT OF
C THE EXTERNAL FUNCTION FCT IN THE DIRECTION OF DECREASING VALUE
C OF THE FUNCTION UNTIL A NEGATIVE VALUE IS ENCOUNTERED.  CONTROL
C IS THEN RETURNED TO THE MAIN PROGRAM.
      COMMON DE(3),XNEO,TEO,XAB(3),PH,PA,P,V,SIG13,FLX,FF,SIG1,B11,B2,GA
     -N,SIG4
      J1=0
      I1=0
      TE1=TEO
      TE=1.01*TEO
      S=FCT(TEO)
      S1=FCT(TE)
```

```
      IF (S1)1027,999,999
 999  IF (S-S1)1000,1000,1005
  998 TE1=TEO
 1000 TE=TE1/1.01
      S=FCT(TE)
      IF (S)1027,1007,1007
1007  I1=I1+1
      IF (I1-800)1001,1001,1002
 1002 IF (J1-800)997,997,1027
 1001 TE1=TE
      GO TO 1000
 997  TE1=TEO
 1005 TE=TE1*1.01
      S=FCT(TE)
      IF(S) 1027,1003,1003
 1003 J1=J1+1
      IF (J1-800)1006,1006,1004
 1004 IF (I1-800)998,998,1027
1006  TE1=TE
      GO TO 1005
1027  XLI=TEO
      XRI=TE
      RETURN
      END


      SUBROUTINE NPOS(S,S1,XRI,XLI)
C     THIS SUBROUTINE SEARCHES FOR THE RIGHT-HAND BOUNDARY USED
C BY RTMI IN SOLVING THE ELECTRON DENSITY CONTINUITY EQUQTION.
C     THE SEARCH IS PERFORMED BY INCREMENTING THE ARGUMENT OF
C THE EXTERNAL FUNCTION FCN IN THE DIRECTION OF INCREASING VALUE
C OF THE FUNCTION UNTIL A POSITIVE VALUE IS ENCOUNTERED.  CONTROL
C IS THEN RETURNED TO THE MAIN PROGRAM.
      COMMON DE(3),XNEO,TEO,XAB(3),PH,PA,P,V,SIG13,FLX,FF,SIG1,B1I,B2
     -E,SIG4
      J1=0
      I1=0
      XNE=1.01*XNEO
      XNE1=XNEO
      S=FCN(XNEO)
      S1=FCN(XNE)
      IF (S1)11,11,28
  11  IF (S-S1)17,12,12
  7   XNE1=XNEO
  12  XNE=XNE1/1.01
      S=FCN(XNE)
      IF(S)10,10,28
  10  I1=I1+1
      IF (I1-1000)13,13,8
  8   IF(J1-1000)6,6,28
  13  XNE1=XNE
      GO TO 12
  6   XNE1=XNEO
  17  XNE=XNE1*1.01
```

```
      S=FCN(XNE)
      IF(S)16,16,28
   16 J1=J1+1
      IF (J1-1000)18,18,19
   19 IF(I1-1000)7,7,28
   18 XNE1=XNE
      GO TO 17
   28 XRI=XNE
      XLI=XNEO
      RETURN
      END


      SUBROUTINE NNEG(S,S1,XRI,XLI)
C     THIS SUBROUTINE SEARCHES FOR THE LEFT-HAND BOUNDARY USED
C BY RTMI IN SOLVING THE ELECTRON DENSITY CONTINUITY EQUQTION.
C     THE SEARCH IS PERFORMED BY INCREMENTING THE ARGUMENT OF
C THE EXTERNAL FUNCTION FCT IN THE DIRECTION OF DECREASING VALUE
C OF THE FUNCTION UNTIL A NEGATIVE VALUE IS ENCOUNTERED.  CONTROL
C IS THEN RETURNED TO THE MAIN PROGRAM.
      COMMON DE(3),XNEO,TEO,XAB(3),PH,PA,P,V,SIG13,FLX,FF,SIG1,B11,B2,GA
     -M,SIG4
      J1=0
      I1=0
      XNE=1.01*XNEO
      XNE1=XNEO
      S=FCN(XNEO)
      S1=FCN(XNE)
      IF (S1)27,9,9
    9 IF (S-S1)10,10,15
    7 XNE1=XNEO
   10 XNE=XNE1/1.01
      S=FCN(XNE)
      IF (S)27,14,14
   14 I1=I1+1
      IF (I1-1000)11,11,13
   13 IF(J1-1000)8,8,27
   11 XNE1=XNE
   12 GO TO 10
    8 XNE1=XNEO
   15 XNE=XNE1*1.01
      S=FCN(XNE)
      IF (S)27,18,18
   18 J1=J1+1
      IF (J1-1000)16,16,17
   17 IF(I1-1000)7,7,27
   16 XNE1=XNE
      GO TO 15
   27 XRI=XNE
      XLI=XNEO
      RETURN
      END
```

```
      FUNCTION FCT(TEN)
C     EXTERNAL FUNCTION USED BY RTMI IN SOLVING ENERGY BALANCE
C EQUATION
      COMMON DE(3),XNEO,TEO,XAB(3),PH,PA,P,V,SIG13,FLX,FF,SIG1,B11,B2,GA
     -M,SIG4
      ALFD=9.1E-7*(300./TEN)**.61
      ALF9=4.0E-20*(300./TEN)**4*XNEO+1.8E-10*(300./TEN)*P
      ALF12=7.0E-11*SQRT(TEN)
      AA10=B11-(27.3*ALF9*PH*PH*B11*XNEO/(78*PH*PH+3.55E-1*V*PA)/(ALF9*X
     -NEO+2.2E-10*3.55E16*PA+2.4E-29*1.26025E33*PH*PA))
      BB10=1.491E6*PA+ALF12*XNEO+.6*PH*PH
      CC10=-SIG13*FLX*3.55E16*PH*FF/.56-(54.6*ALF9*PH*PH*SIG13*FLX*3.55E
     -16*PH*FF*XNEO/(78*PH*PH+3.55E-1*V*PA)/(ALF9*XNEO+2.2E-10*3.55E16*P
      CC10=-SIG13*FLX*3.55E16*PH*FF/.56-(54.6*ALF9*PH*PH*SIG13*FLX*3.55E
     -A+2.4E-29*1.26025E33*PA*PH))
      C10=(-BB10+SQRT(BB10**2-4*AA10*CC10))/2/AA10
      XXX=SIG13*FLX*FF*3.55E16*PH*DE(1)-1.74E-17*ABS(TEN-300.)*SQRT(TEN)
     -*3.55E16*P*XNEO+9E-10*C10**2*DE(2)+7E-11*DE(3)*C10*XNEO*SQRT(TEN)
      FCT=XXX/1.E15
      RETURN
      END


      FUNCTION FCN(XNEN)
C     EXTERNAL FUNCTION USED BY RTMI IN SOLVING ELECTRON DENSITY
C CONTINUITY EQUATION
      COMMON DE(3),XNEO,TEO,XAB(3),PH,PA,P,V,SIG13,FLX,FF,SIG1,B11,B2,GA
     -M,SIG4
      ALFD=9.1E-7*(300./TEO)**.61
      ALF9=4.0E-20*(300./TEO)**4*XNEN+1.8E-10*(300./TEO)*P
      ALF12=7.0E-11*SQRT(TEO)
      C1=SIG13*FLX*3.55E16*PH*FF/(78.*PH**2+SIG1*V*3.55E16*PA)
      C2=.5*B11/(78.*PH**2+SIG1*V*3.55E16*PA)
      C3=78*PH**2/(B2*3.55E16*PA+GAM*1.26025E33*PA*PH+ALF9*XNEN)
      C4=(SIG1*V*3.55E16*PA+(B2+GAM*3.55E16*PH)*3.55E16*PA*C3)/(ALF9*XNE
     -N+376.*PH*PA)
      C5=SIG4*V*3.55E16*PA/(ALF9*XNEN+376.*PA*PH)
      AA10=B11-(27.3*ALF9*PH*PH*B11*XNEN/(78*PH*PH+3.55E-1*V*PA)/(ALF9*X
     -NEN+2.2E-10*3.55E16*PA+2.4E-29*1.26025E33*PH*PA))
      BB10=1.491E6*PA+ALF12*XNEN+.6*PH*PH
      CC10=-SIG13*FLX*3.55E16*PH*FF/.56-(54.6*ALF9*PH*PH*SIG13*FLX*3.55E
     -16*PH*FF*XNEN/(78*PH*PH+3.55E-1*V*PA)/(ALF9*XNEN+2.2E-10*3.55E16*P
     -A+2.4E-29*1.26025E33*PA*PH))
      C10=(-BB10+SQRT(BB10**2-4*AA10*CC10))/2/AA10
     -A+2.4E-29*1.26025E33*PA*PH))
      HEI=C1+C2*C10*C10
      HEII=C3*HEI
      ARI=C4*HEI+C5*C10
      ARX=ALF9*ARI*XNEN/(2.E-9*3.55E16*PA+(    (ALF9*XNEN)))
      ARII=(2.E-9*ARX*3.55E16*PA+376.*PH*PA*ARI)/(ALFD*XNEN)
      YYY=HEI+HEII+ARI+ARII-XNEN
      FCN=YYY/1.E15
      RETURN
      END
```

REFERENCES

1. Jalufka, N. W., DeYoung, R.J., Hohl, F. and Williams, M.D. "Nuclear-Pumped ^{3}He-Ar laser excited by the $^{3}He(n,p)^{3}H$ Reaction", Applied Physics Letters, Vol. 29, No. 3, (August 1 1976), pp.188-190.

2. Harries, W.L. and Wilson, J.W. "Simplified model of a Volumetric Direct Nuclear Pumped ^{3}He-Ar Laser", Proceedings of the First International Symposium on Radiation Induced Plasmas and Nuclear Pumped Lasers. May 23-25, 1978, Orsay, France

3. Biondi, M.A., and Shiu, Y. J., "Dissociative Recombination in Argon: Dependence of the Total Rate Coefficient and Excited-State Production on Electron Temperature", Physical Review, Vol. 17, No. 3 (March 1978), p. 868.

4. Frommhold, L., and Biondi, M. A., "Interferometric Study of Dissociative Recombination Radiation and Argo Afterglows", Physical Review, Vol. 185, No. 1, (September 5, 1969), pp.244-252.

5. Whitten, B. L., Downes L. W. and Wells, W. E., "Collisional Radiative Recombination in High Pressure Noble Gas Mixtures", Proccedings of the First International Symposium on Nuclear Induced Plasmas and Nuclear Pumped Lasers, (May 23-25, 1978) Orsay, France.

6. DeYoung, R. D., Jalufka, N. W. , and Hohl, F., "Direct Nuclear Pumped Lasers Using the $^{3}He(n,p)^{3}H$ Reaction", AIAA Journal, Vol. 16, No. 9, (September 1978), pp.991-999

7. Ortec Publication No. 2687 (ML581) 03C 0976

8. Monchicourt, P., Deloche, R., Wells, W.E., and Berlande, J., "Electron

Radiation Temperature Measurements in a Helium Afterglow at 300 K", Journal de Physique, Vol. 6, (Sept. 1973), pp. 1881-1891

9. DePaola, B. D., Marcum, S.D., Wrench, H.K., Whitten, B.L., and Wells, W.E., "Estimations of Electron Densities and Temperatures in ^{3}He-Dominated Plasmas", Proccedings of The First International Symposium on Nuclear Induced Plasmas and Nuclear Pumped Lasers, (May 23-25, 1978) Orsay, France

NASA
FORMAL
REPORT

FFNo 665 Aug 65